



Green Edge ice camp campaigns: understanding the processes controlling the under-ice Arctic phytoplankton spring bloom

Philippe Massicotte^{1,3}, Rémi Amiraux^{1,2,3}, Marie-Pier Amyot¹, Philippe Archambault^{1,3}, Mathieu Ardyna^{4,5}, Laurent Arnaud⁶, Lise Artigue⁷, Cyril Aubry^{1,3}, Pierre Ayotte^{8,9,10}, Guislain Béchu¹, Simon Bélanger^{11,3}, Ronald Benner¹², Henry C. Bittig^{4,13}, Annick Bricaud⁴, Éric Brossier¹⁴, Flavienne Bruyant¹, Laurent Chauvaud², Debra Christiansen-Stowe¹⁵, Hervé Clastre⁴, Véronique Cornet-Barthaux¹⁶, Pierre Coupel¹, Christine Cox¹⁴, Aurelie Delaforge¹⁷, Thibaud Dezutter^{1,3}, Céline Dimier¹⁸, Florent Domine¹, Francis Dufour¹, Christiane Dufresne^{19,19,3}, Dany Dumont^{19,19,3}, Jens Ehn¹⁷, Brent Else²⁰, Joannie Ferland¹, Marie-Hélène Forget¹, Louis Fortier^{1,3}, Martí Galí^{1,21}, Virginie Galindo^{19,3}, Morgane Gallinari², Nicole Garcia¹⁶, Catherine Gérikas Ribeiro^{22,23}, Margaux Gourdal¹, Priscilla Gourvil²⁴, Clemence Goyens²⁵, Pierre-Luc Grondin¹, Pascal Guillot^{26,3}, Caroline Guilmette¹, Marie-Noëlle Houssais²⁷, Fabien Joux²⁸, Léo Lacour¹, Thomas Lacour²⁹, Augustin Lafond¹⁶, José Lagunas¹, Catherine Lalande¹, Julien Laliberté¹, Simon Lambert-Girard¹, Jade Larivière¹, Johann Lavaud¹, Anita LeBaron¹, Karine Leblanc¹⁶, Florence Le Gall²², Justine Legras¹⁶, Mélanie Lemire^{8,30,10,3}, Maurice Levasseur^{1,3}, Edouard Leymarie⁴, Aude Leynaert², Adriana Lopes dos Santos³¹, Antonio Lourenço²⁷, David Mah³¹, Claudie Marec^{1,32}, Dominique Marie²², Nicolas Martin²⁷, Constance Marty¹⁴, Sabine Marty³³, Guillaume Massé¹, Atsushi Matsuoka¹, Lisa Matthes¹⁷, Brivaela Moriceau², Pierre-Emmanuel Muller¹⁴, Christopher-John Mundy¹⁷, Griet Neukermans^{1,4}, Laurent Oziel^{1,4}, Christos Panagiotopoulos¹⁶, Jean-Jacques Pangrazi¹⁴, Ghislain Picard³⁴, Marc Picheral⁴, France Pinczon du Sel¹⁴, Nicole Pogorzelec¹⁷, Ian Probert²⁴, Bernard Quéguiner¹⁶, Patrick Raimbault¹⁶, Joséphine Ras⁴, Eric Rehm¹, Erin Reimer¹, Jean-François Rontani¹⁶, Søren Rysgaard¹⁷, Blanche Saint-Béat^{1,3}, Makoto Sampei³⁵, Julie Sansoulet¹, Catherine Schmechtig³⁶, Sabine Schmidt³⁷, Richard Sempéré¹⁶, Caroline Sévigny³⁸, Yuan Shen^{39,a}, Margot Tragin²², Jean-Éric Tremblay^{1,3}, Daniel Vaulot^{22,31}, Gauthier Verin¹, Frédéric Vivier²⁷, Anda Vladoiu^{27,40}, Jeremy Whitehead²⁰, and Marcel Babin¹

¹TSI UMI Takuvik, CNRS/Université Laval, Québec G1V 0A6, QC, Canada

²LEMAR, Univ Brest, CNRS, IRD, Ifremer, 29280 Plouzane, France

³Québec-Océan, Université Laval, Québec G1V 0A6, QC, Canada

⁴Laboratoire d'Océanographie de Villefranche, Sorbonne Université, CNRS, LOV, 06230 Villefranche-sur-Mer, France

⁵Department of Earth System Science, Stanford University, Stanford, CA 94305, USA

⁶UMR 5001, IGE, CNRS, 40700 Grenoble, France

⁷LEGOS, University of Toulouse, CNRS, CNES, IRD, UPS, 31400 Toulouse, France

⁸Axe Santé des populations et pratiques optimales en santé, Centre de recherche du CHU de Québec – Université Laval, Québec G1S 4L8, QC, Canada

⁹Centre de toxicologie du Québec, INSPQ, Québec G1V 5B3, QC, Canada

¹⁰Département de médecine sociale et préventive, Université Laval, Québec G1V 0A6, QC, Canada

¹¹Département de Biologie, Chimie et Géographie (groupes BORÉAS et Québec-Océan), Université du Québec à Rimouski, 300 allée des Ursulines, Rimouski G5L 3A1, QC, Canada

¹²Department of Biological sciences, University of South Carolina, Columbia, SC 29208, USA

¹³Leibniz Institute for Baltic Sea Research Warnemünde, IOW, Rostock-Warnemünde, Germany

- ¹⁴Independent researcher, 8 rue Maison Dieu, 75014 Paris, France
- ¹⁵Institut nordique du Québec, Université Laval, Québec G1V 0A6, QC, Canada
- ¹⁶Mediterranean Institute of Oceanography (MIO), Aix-Marseille Université, Université de Toulon, CNRS, IRD, UM110, 13288 Marseille, France
- ¹⁷Centre for Earth Observation Science, University of Manitoba, Winnipeg R3T 2N2, MB, Canada
- ¹⁸FR3761, Institut de la Mer de Villefranche, CNRS, 06230 Villefranche-sur-Mer, France
- ¹⁹Institut des sciences de la mer de Rimouski, Université du Québec à Rimouski, 300 allée des Ursulines, Rimouski G5L 3A1, QC, Canada
- ²⁰Department of Geography, University of Calgary, Calgary T2N 1N4, AB, Canada
- ²¹Barcelona Supercomputing Center (BSC), Barcelona, Spain
- ²²CNRS, Sorbonne Université, UMR7144, Team ECOMAP, Station Biologique de Roscoff, 29680 Roscoff, France
- ²³GEMA Center for Genomics, Ecology & Environment, Faculty of Sciences, Universidad Mayor, Camino La Pirámide 5750, 8580745 Santiago, Chile
- ²⁴Station Biologique de Roscoff (FR 2424), Sorbonne Université, CNRS, Centre de Ressources Biologiques Marines, 29680 Roscoff, France
- ²⁵Operational Directorate Natural Environment, Royal Belgian Institute of Natural Sciences (RBINS), 29 Rue Vautierstraat, 1000 Brussels, Belgium
- ²⁶Amundsen Science, Université Laval, Rimouski G1V 0A6, QC, Canada
- ²⁷Laboratoire d'Océanographie et du Climat, CNRS, IRD, MNHN, Sorbonne Université, 4 place Jussieu, 75005 Paris, France
- ²⁸Sorbonne Université, CNRS, Laboratoire d'Océanographie Microbienne (LOMIC), Observatoire Océanologique de Banyuls, 66650 Banyuls-sur-mer, France
- ²⁹IFREMER, Physiology and Biotechnology of Algae Laboratory, rue de l'Ile d'Yeu, 44311 Nantes, France
- ³⁰Institut de biologie intégrative et des systèmes, Université Laval, Québec G1V 0A6, QC, Canada
- ³¹Asian School of the Environment, Nanyang Technological University, 50 Nanyang Avenue, Singapore 639798, Singapore
- ³²Univ. Brest, CNRS, IUEM, UMS3113, 29280 Plouzane, France
- ³³Norwegian institute for water research, Gaustadalleen 21, 0349 Oslo, Norway
- ³⁴Institut des Géosciences de l'Environnement, 54 rue Molière, 38402 Saint Martin d'Hères, France
- ³⁵Faculty of fisheries sciences, Hokkaido University, Hakodate, Japan
- ³⁶OSU Ecce Terra – UMS 3455, Sorbonne Université, 4 place Jussieu, 75252 Paris CEDEX 05, France
- ³⁷UMR 5805 EPOC, OASU, Université de Bordeaux, 33615 Pessac, France
- ³⁸Environnement et changement climatique Canada, 1550 Avenue D'Estimauville, Québec G1J 0C3, QC, Canada
- ³⁹School of the Earth, Ocean and Environment, University of South Carolina, Columbia, SC 29208, USA
- ⁴⁰Applied Physics Laboratory, University of Washington, Seattle, WA 98105, USA
- ^apresent address: Ocean Sciences Department, University of California, Santa Cruz, CA 95064, USA

Correspondence: Philippe Massicotte (philippe.massicotte@takuvik.ulaval.ca)

Received: 4 September 2019 – Discussion started: 11 September 2019

Revised: 18 November 2019 – Accepted: 2 December 2019 – Published:

Abstract. The Green Edge initiative was developed to investigate the processes controlling the primary productivity and fate of organic matter produced during the Arctic phytoplankton spring bloom (PSB) and to determine its role in the ecosystem. Two field campaigns were conducted in 2015 and 2016 at an ice camp located on land-fast sea ice southeast of Qikiqtarjuaq Island in Baffin Bay (67.4797° N, 63.7895° W). During both expeditions, a large suite of physical, chemical and biological variables was measured beneath a consolidated sea-ice cover from the surface to the bottom (at 360 m depth) to better understand the factors driving the PSB. Key variables, such as conservative temperature, absolute salinity, radiance, irradiance, nutrient concentrations, chlorophyll a concentration, bacteria, phytoplankton and zooplankton abundance and taxonomy, and carbon stocks and fluxes were routinely measured at the ice camp. Meteorological and snow-relevant variables were also monitored. Here, we present the results of a joint effort to tidy and standardize the collected datasets, which will facilitate their reuse in other Arctic studies. The dataset is available at <https://doi.org/10.17882/59892> (Massicotte et al., 2019a).

1 Introduction

In the Arctic Ocean, the phytoplankton spring bloom (PSB) initiates the period of highest biomass primary production of the year (Sakshaug, 2004; Perrette et al., 2011; Ardyna et al., 2013). Although it was discovered that the PSB may occur more extensively and more frequently beneath a consolidated ice pack (Arrigo et al., 2012, 2014; Assmy et al., 2017), only a small number of research initiatives (e.g., Fortier et al., 2002; Galindo et al., 2014; Mundy et al., 2009, 2014; Wassmann et al., 1999; Gosselin et al., 1997) have investigated the processes controlling the Arctic PSB in the ice-covered water column. Additionally, ice algal communities play an important role within the Arctic food web and for carbon export to the benthos during the winter–spring transition (Leu et al., 2015). However, primary production within the Arctic ice pack is still poorly understood. The Green Edge project was conceived in an effort to better understand the Arctic PSB from the level of fundamental physical, chemical and biological processes to that of their interactions within the ecosystem and at spatial scales ranging from local to pan-Arctic. Besides studying each major component of the processes controlling Arctic PSB, another objective of Green Edge was to investigate its impact on the nutrients and carbon dynamics within the ecosystem. A total of three Green Edge campaigns were conducted: two ice camp campaigns on landfast sea ice in 2015 and 2016 and an oceanographic cruise aboard the CCGS *Amundsen* in Baffin Bay in 2016. In this article, we present an overview of an extensive and comprehensive dataset acquired during two surveys conducted at the Green Edge ice camp.

2 Study area, environmental conditions and sampling strategy

The field campaigns were conducted on landfast sea ice southeast of Qikiqtarjuaq Island in Baffin Bay (67.4797° N, 63.7895° W, Fig. 1) in 2015 (15 March–17 July) and 2016 (20 April–27 July). These periods were chosen in order to capture the dynamics of the sea-ice algae and phytoplankton spring blooms, from bloom initiation to termination. The field operations took place at a location (the “ice camp”) south of Qikiqtarjuaq Island where the water depth is 360 m. Continuous records of wind speed and air temperature were made with a meteorological station: an automated Meteo Mat equipped with temperature (HC2S3) and wind (05305-L) sensors (Campbell Scientific) positioned near (< 100 m) the tent (Polarhaven, Weatherhaven), in which water sampling was carried out. During the sampling periods, the study site experienced changes in snow cover and ice thickness (Fig. 2). In 2015, the snow and ice thickness at the monitoring spot varied between 2 and 40 cm (mean of 21 cm) and 103 and 136 cm (mean of 121), respectively. In 2016, the snow and

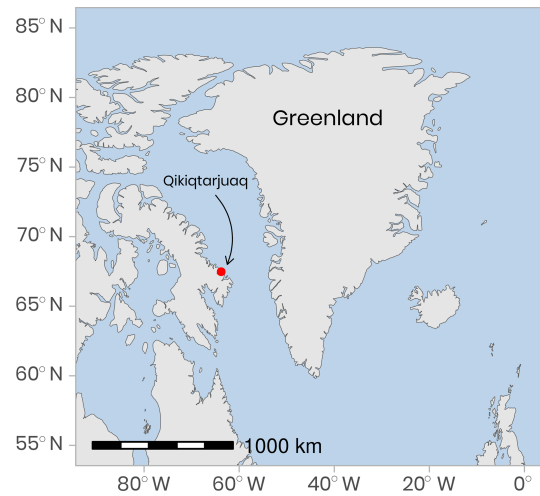


Figure 1. Location of the ice camp located near Qikiqtarjuaq Island in Baffin Bay. The projection used is EPSG-4326.

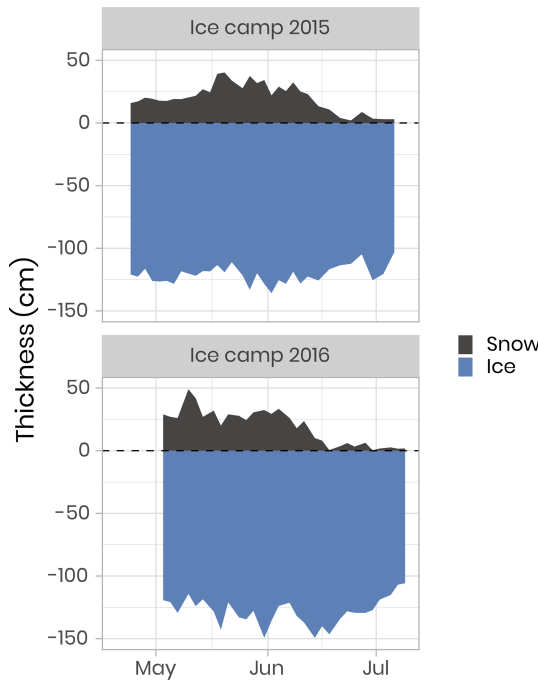
ice thickness varied between 0.3 and 49 cm (mean of 19 cm) and 106 and 149 cm (mean of 128 cm), respectively. For both years, snowmelt began at the beginning of June and lasted for approximately 2 to 3 weeks (Oziel et al., 2019). Water sampling was usually carried out every 2 d through a 1×1 m hole in the ice pack shielded by the tent. For the analysis of nutrient concentrations, photosynthetic parameters, primary production, chlorophyll *a* (chl *a*), phytoplankton taxonomy, and carbon stocks, such as dissolved organic carbon (DOC) and particulate organic carbon (POC); water samples were collected at 1.5, 5, 10, 20, 40 and 60 m using 10 or 20 L Niskin bottles. Details about specific measurements, such as zooplankton and bacteria abundances, are provided in the following sections.

3 Data quality control and data processing

Different quality control procedures were adopted to ensure the integrity of the data. First, the raw data were visually screened to eliminate errors originating from the measurement devices, including sensors (systematic or random) and errors inherent from measurement procedures and methods. Statistical summaries such as average, standard deviation and range were computed to detect and remove anomalous values in the data. Following from this, data were checked for duplicates and remaining outliers. Once raw measurements were cleaned, data were structured and regrouped into plain text comma-separated (CSV) files. Each of these files was constructed to gather variables of the same nature (e.g., nutrients). In each of these files, a minimum number of variables (columns) were always included so the different datasets could be easily merged together (Table 1). More than 120 different variables were measured dur-

Table 1. Descriptions of the minimal variables included in each dataset (i.e., in each CSV file).

Variable	Description
date	Sampling date (UTC)
latitude	Latitude of the sampling location (degree decimals)
longitude	Longitude of the sampling location (degree decimals)
sample_type	Origin of the water (“water”, “ice”, “melt pond”)
sample_source	Source of the water (“niskin”, “underice” “0–1 cm”, “0–3 cm”, “3–10 cm”, “rosette”)
depth_m	Depth at which measurement was made
snow_thickness	Qualitative value describing the snow cover under which measurement was made (“thin_snow”, “thick_snow”)
mission	Mission identifier (“ice_camp_2015”, “ice_camp_2016”)
pi	Name(s) of the principal investigator(s) responsible of the measured variable

**Figure 2.** Temporal evolution of the snow and sea-ice thickness for both ice camp missions. The dashed horizontal line represents the snow–ice interface.

ing the Green Edge landfast-ice expeditions. The complete list of variables is presented in Table 2 and detailed metadata information can be found in the LEFE-CYBER online repository (<http://www.obs-vlfr.fr/proof/php/GREENEDGE/greenedge.php>, last access: 2 December 2019). The processed and tidied version of the data is hosted at SEANOE (SEA scieNtific Open data Edition) under the CC-BY license (<https://www.seanoe.org/data/00487/59892/>, last access: 2 December 2019, Massicotte et al., 2019a). In the following sections, we present a subset of these variables along with the methods used to collect and measure them. For each of these variables, time series or vertical profiles are used to describe the data. Data cleaning and visualization were per-

formed with R 3.6.1 (R Core Team, 2019). The code used to produce the figures and the analysis presented in this paper is available under the GNU GPLv3 license (<https://github.com/PMassicotte/greenedge-icecamp-data-paper>, last access: 2 December 2019). The code used to process and tidy the data provided by each researcher is also publicly available (<https://gitlab.com/Takuvik/greenedge-database>, last access: 2 December 2019) under the GNU GPLv3 license.

4 Data description: an overview

4.1 Physical data

Some meteorological variables were measured during both campaigns. Starting on 27 March 2015, air temperature, relative humidity, wind speed and snow depth were measured. Data were recorded using a CR1000 Campbell data logger. Field measurements were performed most days to obtain snow physical variables. These included vertical profiles of snow density and specific surface area with 1 cm vertical resolution and visual determination of snow stratigraphy. Snow spectral albedo in the 400–1100 nm spectral range was also measured during these field measurements. Snow measurements are detailed in Verin et al. (2019).

Underwater conductivity, conservative temperature and depth (CTD) vertical profiles were measured using a Sea-Bird SBE19plusV2 CTD system (factory-calibrated prior to the expedition) deployed from inside the Polarhaven tent between the surface and a 350 m depth. The data were post-processed according to the standard procedures recommended by the manufacturer and averaged into 1 m vertical bins. During the sampling periods, absolute salinity (S_A) was generally greater than 31.5 g kg^{-1} (range of $4\text{--}34.4 \text{ g kg}^{-1}$). Flushes of freshwater at the ocean surface due to snow and ice melt started slowly at the beginning of June with the largest peaks and pulses taking place late June when absolute salinity decreased to approximately 4 g kg^{-1} (Fig. 3). Note that the new standard of absolute salinity is used for the remainder of this paper (Oziel et al., 2019; Randelhoff et al., 2019).

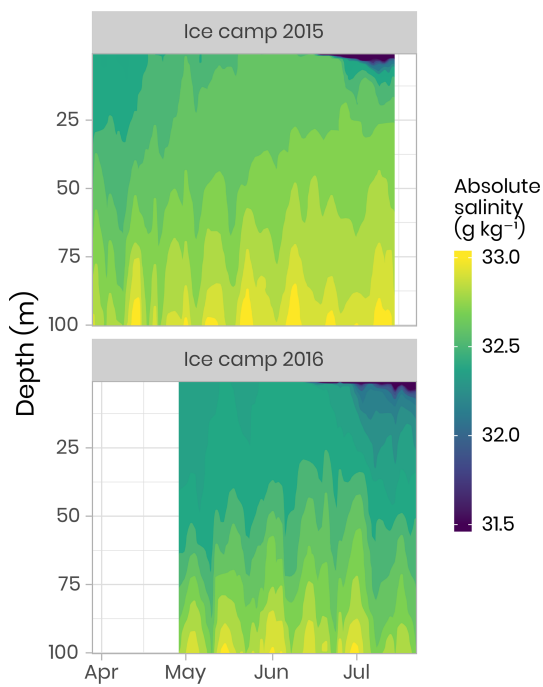


Figure 3. Temporal evolution of the salinity in the first 100 m of the water column for both campaigns. Note that, for visualization purposes, salinity below 31.5 g kg^{-1} has been binned to 31.5 g kg^{-1} . Note that salinity as low as 4 g kg^{-1} was observed during flushes of freshwater at the ocean surface due to snow and ice melt (dark blue color in the figure).

Ocean current profiles in the water column were measured using a downward-looking 300 kHz Sentinel Workhorse Acoustic Doppler Current Profiler (ADCP, RDI Teledyne) mounted directly beneath the sea-ice bottom. The study site was dominated by seawater originating from the Arctic Ocean modulated by spring–neap tidal cycles (14 d) and semidiurnal M2 periods ($\approx 12.4 \text{ h}$). Vertical profiles of water column turbulence were measured on 23 June 2016 during a spring tidal cycle (≈ 12.4) using a self-contained autonomous microprofiler (SCAMP, Precision Measurement Engineering, California, USA). The turbulence profile (i.e., a median profile of the rate of dissipation of turbulent kinetic energy, ϵ) showed a mixing layer depth of about 20–25 m, characterized by an elevated dissipation rate with values above $10^{-8} \text{ W kg}^{-1}$. The reader is referred to the paper by Oziel et al. (2019) for detailed methods, visualization and discussion of the CTD, SCAMP and ADCP data.

Vertical profiles (surface to 200 m) of CTD and bio-optical properties were measured every hour during a M2 tidal cycle on 9 June 2016 (an example of modeled surface tidal height vs. time is shown in Fig. A1). These observations (Fig. 4) illustrate that internal tidal waves caused large vertical isopycnal displacements (20–30 m) of all observed physical and biogeochemical properties below 50 m depth across the semidiurnal M2 period. Hence, as vertical profiles of

physical and bio-optical variables were measured at approximately the same time each day, properties (assuming they follow a conservative mixing behavior) will appear to be vertically displaced. Therefore, when comparing properties from vertical profiles taken at the ice camp, we suggest that comparisons of profile variables should be made on isopycnal (constant density) coordinates, rather than depth coordinates (Fig. 4).

4.2 Underwater bio-optical data

4.2.1 Radiance and irradiance measurements with ICE-Pro

A total of 173 and 89 vertical radiometric profiles were measured in 2015 and 2016, respectively, using a factory-calibrated ICE-Pro (an ice floe version of the Compact-Optical Profiling System, C-OPS, from Biospherical Instruments Inc.). The ICE-Pro was equipped with radiometers for both downward plane irradiance ($E_d, \text{W m}^{-2} \text{ nm}^{-1}$) and either upward irradiance ($E_u, \text{W m}^{-2} \text{ nm}^{-1}$) in 2015 or upward radiance ($L_u, \text{W m}^{-2} \text{ sr}^{-1} \text{ nm}^{-1}$) in 2016. The profiles were taken at two sites, separated by approximately 40 m. In order to perform the profiles, the ICE-Pro was deployed through auger holes that had been drilled at distances of 82 and 113 m from the tent and cleaned of ice chunks. Once the ICE-Pro was underneath the ice layer, fresh clean snow was shoveled back into the hole to avoid, as much as possible, having a bright spot above the sensors (see Fig. B1 and Table B1). The frame was then manually lowered at a rate of approximately 0.3 m s^{-1} . The above-surface reference sensor was fixed on a steady tripod installed approximately 2 m above the ice surface and above all neighboring camp features. Data processing and validation were performed using a protocol inspired by that of Smith and Baker (1984), which is now used by several space agencies for their Ocean Color algorithm validation activities. Measurements were taken between 380 and 875 nm at 19 discrete spectral wavebands. Vertical profiles were usually performed in duplicates or triplicates. Time series of daily photosynthetically active radiation (PAR, computed from the 19 spectral irradiance wavelengths) at the sea-ice–water interface (1.3 m depth) are shown in Fig. 5. In 2016, PAR started to increase rapidly in the second week of May, compared to early June in 2015. Overall, PAR at 1.3 m in the water column was also greater in 2016 than in 2015 and reached the threshold of $0.415 \text{ mol of photons m}^{-2} \text{ d}^{-1}$, above which light is sufficient for net growth (Letelier et al., 2004), a few days earlier. Further information about in situ underwater irradiance and radiance measurements can be found in Massicotte et al. (2018).

4.2.2 Underwater photos and videos of the ice bottom

Several vertical profiles up to 30 m were performed using a GoPro Hero 4 camera mounted on the ICE-Pro and pointing upwards towards the ice bottom (see Fig. B1 and Table B1).

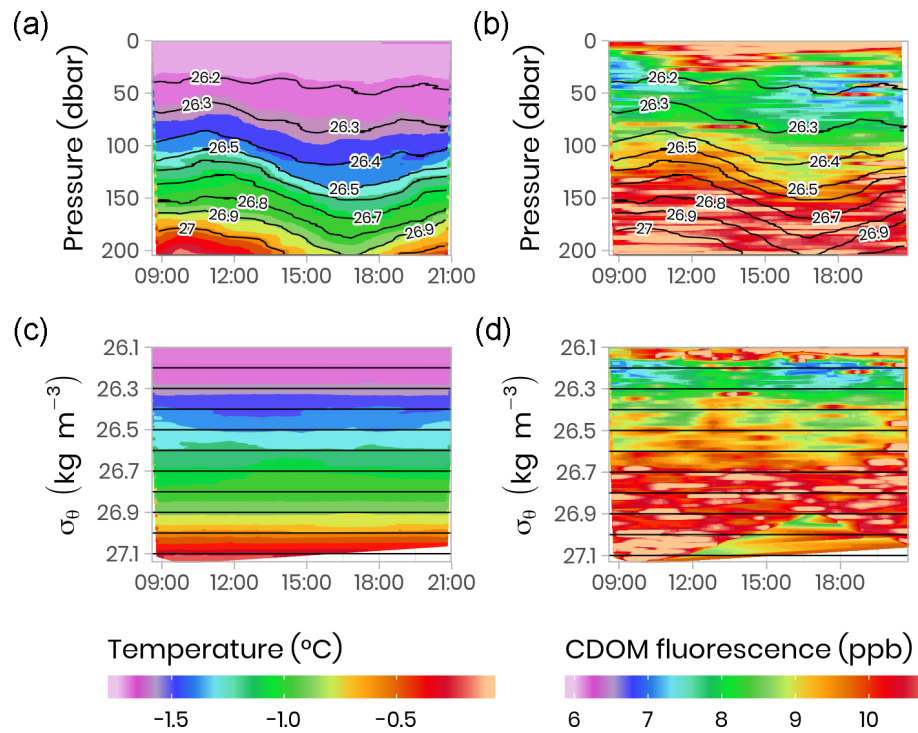


Figure 4. Temporal evolution of physical (temperature) and bio-optical (CDOM fluorescence) variables with superimposed lines of potential density anomaly (σ_θ , kg m^{-3}) during a 13 h tidal cycle. Surface tidal height vs. time at Qikiqtarjuaq is shown in blue. **(a, b)** Plotted vs. pressure coordinates (equivalent to depth in meters). **(c, d)** The same data plotted vs. potential density anomaly σ_θ coordinates (kg m^{-3}). The tidal survey was performed on 9 June 2015.

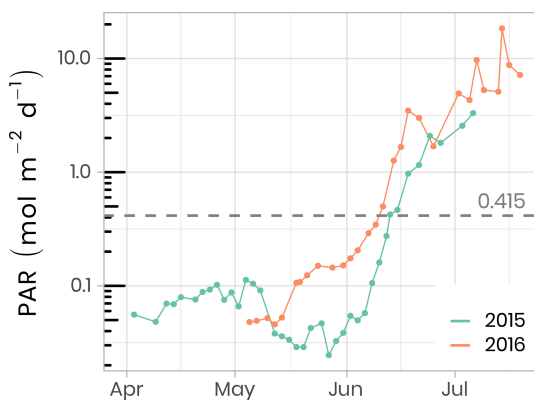


Figure 5. Temporal evolution of daily photosynthetically available radiation (PAR) at the sea-ice–water interface (1.3 m depth) for both ice camp missions. The dashed horizontal line shows the $0.415 \text{ mol photons m}^{-2} \text{ d}^{-1}$ threshold often used in the literature as the minimum light requirement for primary production.

Still images were captured every 5 s during the descent, and a video was taken of the complete descent. These photos and videos were used for a qualitative assessment of the pronounced spatial and temporal heterogeneity of the under-ice environment and the associated water column nekton community between the two profiling locations.

4.2.3 Irradiance measurements with TriOS

To quantify the impact of the heterogeneous radiation field under sea ice on irradiance measurements, replicated spectral irradiance profiles were collected beneath landfast sea ice from 5 May to 8 June 2015 and from 14 June to 4 July 2016. The replicates were made on each sampling day, under different surface conditions. In 2015, measurements were performed prior to melt onset, under different snow depths. In 2016, measurements began after the onset of snowmelt and were performed beneath sea ice with a wet snow cover, shallow melt ponds and white ice. The deployed sensor array consisted of a surface reference radiometer, which recorded incident downwelling planar irradiance, $E_d(0, \phi)$, and three radiometers attached to a custom-built double-hinged aluminum pole (under-ice L-arm) to measure downwelling planar irradiance, $E_d(z, \phi)$, downwelling scalar irradiance, $\dot{E}_d(z, \phi)$, and upwelling scalar irradiance, $\dot{E}_u(z, \phi)$. These four hyperspectral radiometers (two planar RAMSES-ACC and two scalar RAMSES-ASC, TriOS GmbH, Germany) measured pressure and tilt internally and recorded irradiance spectra in the wavelength range from 320 to 950 nm at a resolution of 3.3 nm (190 channels). Transmitted irradiance was recorded along with vertical profiles by lowering the L-arm manually through a 20 cm auger hole with a winch and 1.5 m aluminum poles extensions. In 2015, 17 vertical

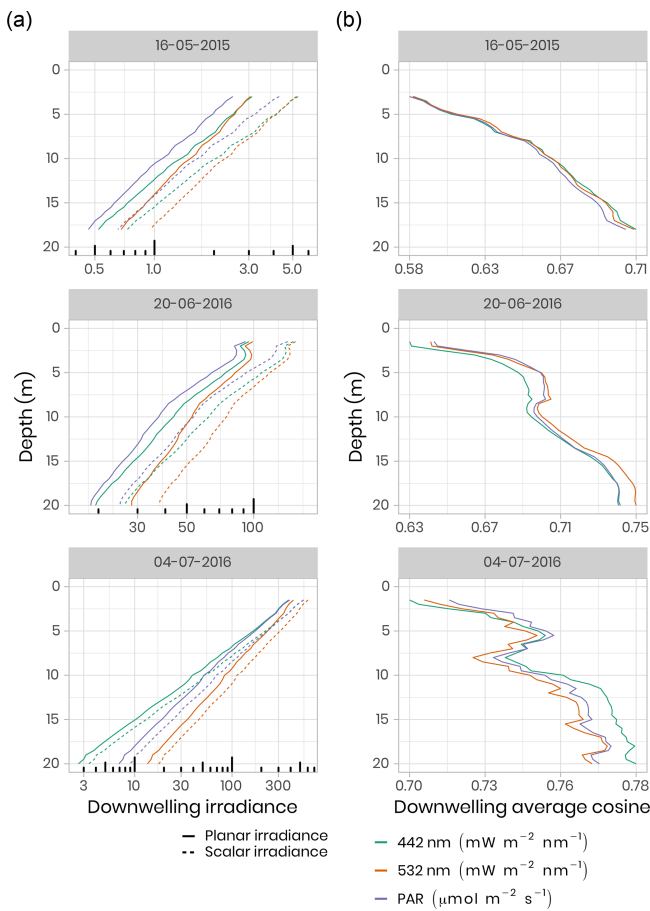


Figure 6. (a) Under-ice vertical profiles of downwelling planar and scalar irradiance at 442 nm and 532 nm and for PAR. Note the log scale for the irradiance measurements. (b) Calculated downwelling average cosine (unitless) was measured beneath snow-covered sea ice on 16 May 2015, beneath bare ice on 20 June 2016 and beneath a melt pond on 4 July 2016.

profiles were collected in 0.4–0.5 m depth steps from the ice bottom to a water depth of 18 m. In 2016, 11 profiles were recorded to a depth of 20 m under different sea-ice surface conditions. Differences between planar and scalar PAR measurements were used to derive the downwelling average cosine, μ_d , an index of the angular structure of the downwelling under-ice radiation field which, in practice, can be used to convert between downwelling scalar, \dot{E}_d , and planar, E_d , irradiance. The average cosine was smaller prior to snowmelt in 2015 compared to after snowmelt (≈ 0.6 vs. 0.7), when melt ponds covered the ice surface in 2016 (Fig. 6). Further details about the sampling procedure, data processing and results can be found in Matthes et al. (2019).

4.2.4 Inherent optical properties (IOPs)

IOP measurements were made using an optical frame equipped with the physical and bio-optical sensors that were

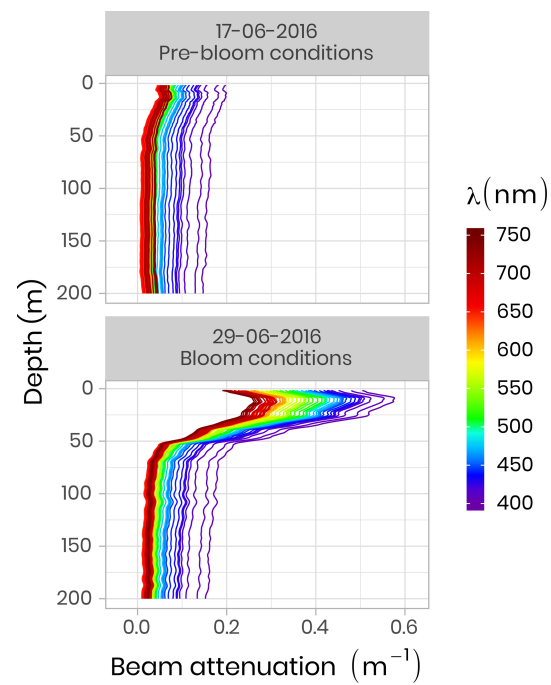


Figure 7. Beam attenuation coefficients (c , m^{-1}) measured in 2016 using a WetLabs AC-S before and during the phytoplankton bloom. Note that the colors of the lines correspond to wavelength frequencies.

factory-calibrated before each field campaign. A Seabird SBE-9 CTD measured temperature, absolute salinity and pressure. A WetLabs AC-S was used for spectral beam attenuation (c , m^{-1}) and total absorption (a , m^{-1}) between 405 and 740 nm, and a BB9 (WetLabs) and BB3 (WetLabs) were utilized for backscattering coefficients (b , m^{-1}) between 440 and 870 nm. During both campaigns, pure water calibration was performed for the AC-S sensor on each sampling day and linear regression of these calibration values as a function of time was computed for each wavelength of absorption and attenuation signals. Following from this, the offset applied during the data processing was taken on this linear regression at the exact date of the measurement. Figure 7 shows two vertical profiles of attenuation coefficients at different wavelengths acquired during pre-bloom and bloom conditions in 2016. One can see that during the bloom, attenuation increased markedly in the 0–50 m surface layer due to higher phytoplankton biomass.

4.2.5 Other optical measurements

Other optical variables measured during both field campaigns included absorbance of particulate matter, absorbance of dissolved organic matter, snow and sea-ice transmittance, snow and ice hyperspectral and hyper-angular hemispherical directional reflectance (Goyens et al., 2018), and surface spectral albedo (Verin et al., 2019) (Table 2). Downwelling

spectral irradiance above the surface ($1^\circ \times 1^\circ$ spatial resolution, daily temporal resolution, interpolated hourly) was also computed based on the radiative transfer model SBDART (Ricchiazzi et al., 1998), as described in Laliberté et al. (2016) and Randelhoff et al. (2019).

4.3 Nutrients and carbon compounds

Nitrate, nitrite, phosphate and silicate concentrations were measured from water filtered through $0.7\text{ }\mu\text{m}$ Whatman GF/F filters and through $0.2\text{ }\mu\text{m}$ cellulose acetate membranes. Filtrates were collected into sterile 20 mL polyethylene vials, poisoned with $100\text{ }\mu\text{L}$ of mercuric chloride (60 mg L^{-1}) and subsequently stored in the dark prior to analysis. Nutrient concentrations were determined using an automated colorimetric procedure described in Aminot and Kérouel (2007). Figure 8 shows an overview of the dynamics of nitrate, which is often the limiting nutrient for phytoplankton growth in the ocean (Tremblay and Gagnon, 2009). It can be seen that the depletion of the nitrate started in approximately mid-June for both years, coinciding with the initiation of the phytoplankton bloom. However, the depletion was observed deeper in the water column in 2016 compared to 2015 due to stronger currents and a longer sampling period in 2016 (Oziel et al., 2019). Dissolved organic and inorganic carbon (DOC and DIC, respectively), particulate organic and inorganic carbon (POC and PIC, respectively), total organic carbon (TOC), phosphate (PO_4), orthosilicic acid (Si(OH)_4), and ammonium (NH_4), were also measured during both campaigns (Table 2). Detailed information about analytical procedures can be found in the LEFE-CYBER online repository. A comprehensive discussion about nutrient dynamics during the Green Edge missions can be found in Grondin et al. (2019).

4.4 Bacteria and phytoplankton

4.4.1 Flow cytometry

The abundances of picophytoplankton, nanophytoplankton and bacteria were measured by flow cytometry. Samples (1.5 mL) were preserved with a mix of glutaraldehyde and Pluronic F-68 (Gibco) (Marie et al., 2014) and frozen at $-80\text{ }^\circ\text{C}$. Samples were analyzed on a FACS Canto flow cytometer (Becton Dickinson) in the laboratory at the Station Biologique de Roscoff. The abundance (cells per milliliter) of phytoplankton populations was determined on unstained samples, and cells were discriminated by their red chlorophyll autofluorescence. Bacterial abundance was determined based on the fluorescence of SYBR green-stained DNA (Marie et al., 1997). In both 2015 and 2016, bacteria concentrations were initially low, on the order of $100\,000$ cells per milliliter, and quite uniform throughout the water column. During the bloom, bacterial abundance increased continuously, reaching values of 1 million cells per milliliter (Fig. 9). Simultaneously, the distribution of highest abundance became stratified with a higher concentration found near the

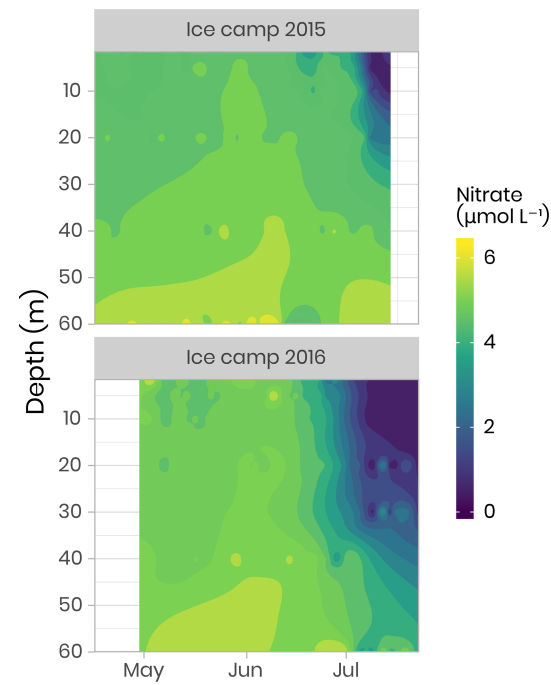


Figure 8. Temporal evolution of nitrate concentrations in the first 60 m of the water column for both ice camp missions.

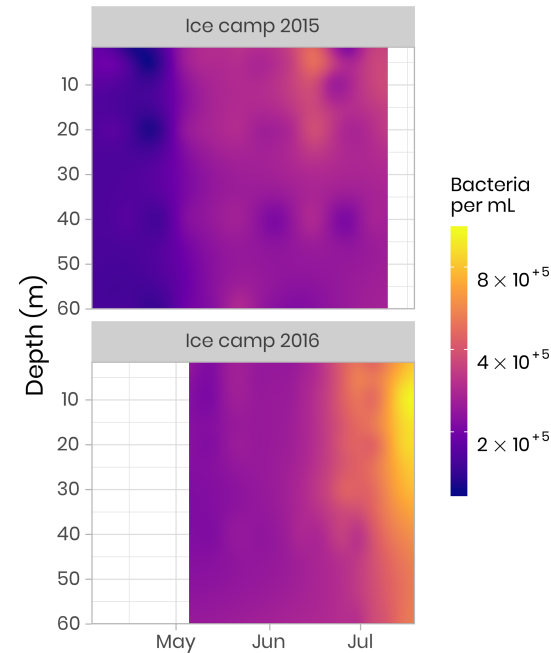


Figure 9. Concentration of bacteria in the water column at the ice camp in 2015 and 2016.

surface in early July before it moved down to the subsurface (between 10 and 20 m) later in July (Fig. 9). In 2015, the sampling period did not extend long enough to capture the full progression of bacterial community development.

4.5 Phytoplankton

4.5.1 Chlorophyll *a*

Chl *a* and accessory pigments concentrations were determined by high-performance liquid chromatography (HPLC) following Ras et al. (2008). Concentrations were measured using volumes between 0.1 and 1 L of melted ice and volumes between 1 and 2.5 L of seawater. Water was filtered onto Whatman GF/F 25 mm filters and stored at -80°C until analysis. Filters were extracted in 100 % methanol, disrupted by sonication and clarified by filtration. Pigments were analyzed using an Agilent Technologies 1200 Series system with a narrow reversed-phase C8 Zorbax Eclipse XDB column ($150 \times 3 \text{ mm}$, $3.5 \mu\text{m}$ particle size), which was maintained at 60°C . Figure 10 shows the temporal evolution of surface integrated chl *a* in the bottom 10 cm of the ice cover and the water column for both years. At the beginning of the sampling periods in 2015 and 2016, total chl *a* concentrations in the bottom of the ice and the water column were of approximately the same magnitude ($\approx 5 \text{ mg m}^{-2}$). Later in the season, when the snowpack and the ice sheet started to melt (between June and July) and at the onset of the PSB, chl *a* in the water column increased rapidly to reach concentrations of 145 mg m^{-2} in 2015 and 113 mg m^{-2} in 2016. At the same time, or slightly before, chl *a* in the ice bottom started to decrease rapidly to concentrations varying between 0.1 and 0.3 mg m^{-2} .

Primary production during the phytoplankton bloom was incompletely sampled in 2015, while in 2016 it was monitored from the onset under melting sea ice in May to its termination in July (Fig. 11). Briefly, rates of carbon fixation (primary production), were measured using a dual ^{13}C – ^{15}N isotopic technique (Raimbault et al., 1999). Water samples and melted ice was collected into three 600 mL polycarbonate bottles, previously rinsed with 10 % HCl and then with ultrapure Milli-Q water. Labeled ^{13}C sodium bicarbonate ($\text{NaH}^{13}\text{CO}_3$ – 6 g, 250 mL^{-1} deionized water – 99 at % ^{13}C , EURISOTOP) was added to each bottle in order to obtain $\approx 9.7\%$ final enrichment (0.5 mL per 580 mL of seawater). After the addition of ^{13}C -tracer (H^{13}CO_3), samples were spiked with inorganic nitrogen labeled with ^{15}N . Immediately after tracer addition, samples were fixed on an array placed under the ice. Incubation was stopped after 24 h and samples were immediately filtered on Whatman GF/F filters (25 mm diameter) precombusted at 500°C . These filters were used to determine the final $^{15}\text{N}/^{13}\text{C}$ enrichment ratio in the particulate organic matter and the concentrations of particulate carbon and particulate nitrogen. During the ice-covered period in 2015, primary production, as well as nitrate assimilation (rNO_3), occurred at very low but detectable rates reaching 8 and $0.4 \text{ mmol m}^{-2} \text{ d}^{-1}$, respectively. Phytoplankton production rates were higher in the ice than in the water column, representing approximately 80 % and 40 % for primary production and rNO_3 , respectively. Estimated assim-

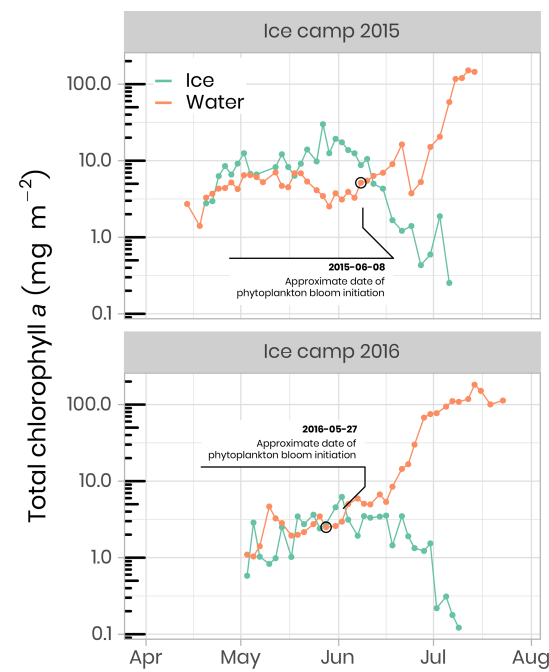


Figure 10. Temporal evolution of chlorophyll *a* in ice and water (depth-integrated) for both ice camp missions. Note that the water chlorophyll *a* have been integrated over the first 100 m of the water column, whereas the ice chlorophyll *a* was measured on the bottom 0–10 cm of the ice cores. The details of the calculations to determine the approximate dates of phytoplankton bloom initiation can be found in Oziel et al. (2019).

ilated concentrations of total carbon and nitrate within the ice cover were 30–96 and $1.4\text{--}4.6 \text{ mmol m}^{-2}$ during this period. The break-up of the sea-ice cover was characterized by a rapid increase in primary production and rNO_3 . During this period of high light transmission through the melting ice cover (day 169 to 190), concentrations of assimilated total carbon and rNO_3 reached 60 and 8 mmol m^{-2} , respectively, leading to a complete nitrate depletion. The quantities of total carbon and nitrate assimilated during the 2016 PSB in the water column were 562 and 97 mmol m^{-2} , respectively.

4.5.2 Phytoplankton taxonomy

The phytoplankton community species composition was determined using an Imaging FlowCytobot (IFCB, Woods Hole Oceanographic Institute, Sosik and Olson, 2007; Olson and Sosik, 2007). The size range targeted was between 1 and $150 \mu\text{m}$, while the image resolution of approximately $3.4 \text{ pixels } \mu\text{m}^{-1}$ limited the identification of cell $< 10 \mu\text{m}$ to broad functional groups. A $150 \mu\text{m}$ Nitex mesh was used to avoid clogging of the fluidics system by large particles, although this might have induced a bias in the results by preventing large cells to be sampled. For each melted ice and seawater sample, 5 mL was analyzed and Milli-Q water was run between samples with high biomass in order

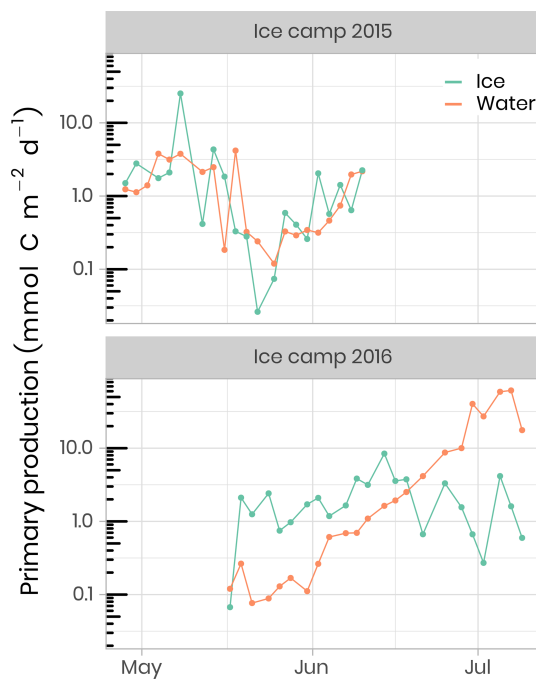


Figure 11. Temporal evolution of primary production in ice and water (depth-integrated) for both ice camp missions.

to prevent contamination between samples. Image acquisition was triggered by chl *a* in vivo fluorescence, with excitation and emission wavelengths of 635 and 680 nm, respectively. Grayscale images were processed to extract regions of interest (ROIs) and their associated features (e.g., geometry, shape, symmetry, texture, etc.), using a custom made MATLAB (2013b) code (Sosik and Olson, 2007; Olson and Sosik, 2007; processing codes are available at <https://github.com/hsosik/ifcb-analysis>, last access: 2 December 2019). A total of 231 features (see the full list and description at <https://github.com/hsosik/ifcb-analysis/wiki/feature-file-documentation>, last access: 2 December 2019) were derived on the resulting ROIs and were used for automatic classification using random forest algorithms with the EcoTaxa application (Picheral et al., 2017). A learning set was manually prepared for each year, with ca. 20 000 images annotated and used for automatic prediction. Each automatically annotated image was further validated by visual examination and corrected when necessary. The final 2015 and 2016 datasets consist of 124 247 and 57 397 annotated images and their associated features in 39 and 35 taxonomic categories, respectively (Fig. 12). As it was impossible to count the number of cells in each image, we assumed one cell per image. To account for potential underestimations of cell abundance when colonies or chains were imaged, the biovolume of each living protist in the images was computed during image processing according to Moberg and Sosik (2012). Using carbon to volume ratios from Menden-Deuer and Lessard (2000), biovolume was converted into carbon estimates, as

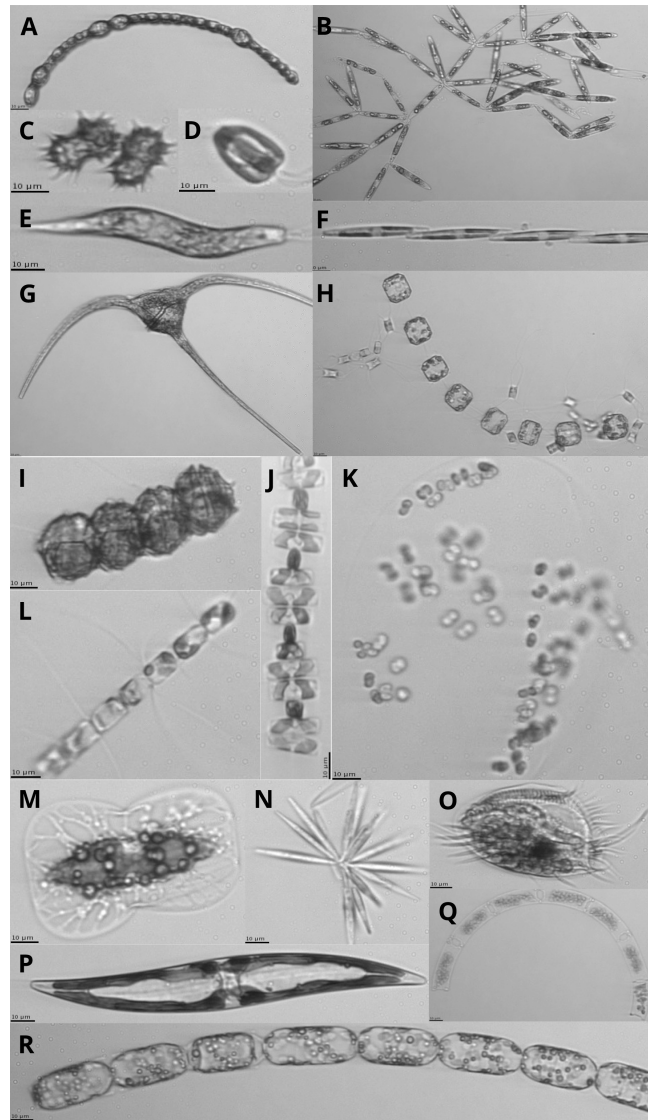


Figure 12. Images of protists sampled with the IFCB (scale bar is 10 µm; note that the images are not to scale): (a) *Anabaena* sp., (b) *Nitzschia frigida*, (c) *Polarella glacialis*, (d) Flagellate, (e) *Euglena*, (f) *Pseudo-nitzschia* sp., (g) *Ceratium* sp., (h) *Thalassiosira nordenskioeldii* with *Attheya septentrionalis*, (i) *Peridiniella catenata*, (j) *Navicula pelagica*, (k) *Phaeocystis* sp. colony, (l) *Chaetoceros* sp., (m) *Entomoneis* sp., (n) *Synedropsis hyperborea*, (o) Ciliate, (p) Pennate diatom, (q) *Eucampia* sp., and (r) *Melosira* sp.

described in Laney and Sosik (2014). Detailed information about sea-ice algae and phytoplankton community composition can be found in Grondin et al. (2019).

4.5.3 Physiology of the phytoplankton community

The photosynthetic potential of microalgae was assessed by measuring F_v/F_m , namely the maximum photochemical efficiency of Photosystem II (PSII), via dynamic chl *a* fluorescence:

$$\frac{F_v}{F_m} = \frac{(F_m - F_0)}{F_m}, \quad (1)$$

where F_m and F_0 are the maximum and minimum PSII chl *a* fluorescence yields, respectively. Chl *a* fluorescence was recorded with a WATER-PAM fluorometer (Heinz Walz GmbH, Germany) on melted sea-ice (last centimeter of the cores) and water samples collected at different depths (i.e., 1.5, 10, 40, 60 m). Measurements were performed after storing samples in 50 mL dark Falcon tubes (Corning Life Sciences, USA) on ice for at least 1 h. For further technical details, see Galindo et al. (2017). F_v/F_m is often used as an index for evaluating the physiological condition of microalgal communities. For algae that are growing optimally, the F_v/F_m ratio ranges between 0.50 and 0.75 in the absence of cyanobacteria. Below 0.50, algal growth is considered to be limited by nutrient availability and/or light stress (Suggett et al., 2010). Figure 13 shows the temporal evolution of F_v/F_m for ice algae and phytoplankton for the ice camp in 2016. At the beginning of the sampling period, all samples showed F_v/F_m above 0.55. While in ice F_v/F_m ranged between 0.60 and 0.75 until the beginning of June, when it decreased to ca. 0.20–0.35 in water. This decrease in F_v/F_m (Fig. 13a) is coincident with a sharp increase in PAR under the ice sheet (Fig. 5), which may have induced light stress in phytoplankton and ice algae communities. After approximately 1 month, phytoplankton became acclimated to this new light environment and F_v/F_m increased back to 0.60–0.75 by the beginning of June. From that time on (corresponding to higher irradiance transmittance through ice; see Fig. 5), F_v/F_m in ice decreased dramatically to an approximate value of 0.20, while F_v/F_m in the water column generally remained between 0.60 and 0.75 for depths between 10 and 60 m (note, however, the large decrease at 40 m on 13 June). In contrast, F_v/F_m at 1.5 m was lower and noisier with values varying between 0.45 and 0.60.

In addition to the photosynthetic potential of microalgae, photosynthetic parameters were measured from seawater incubated at different irradiance levels in the presence of ^{14}C labeled sodium bicarbonate. The light saturation parameter, E_k , is an indication of the light acclimation state of the phytoplankton community. Figure 13b shows the increase in E_k as the phytoplankton community grows between May and July 2016 at 1.5, 5 and 10 m depth. Between 1.5 and 10 m depth, E_k varied between 15 and $194 \mu\text{mol m}^{-2} \text{s}^{-1}$

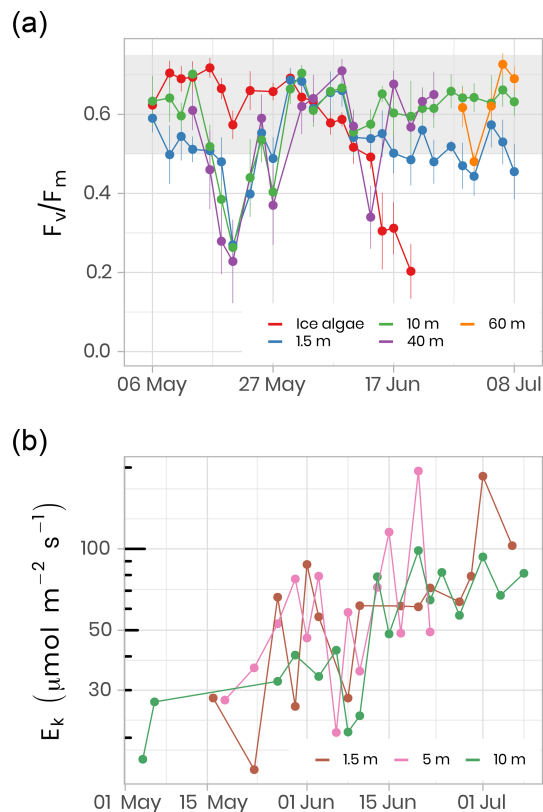


Figure 13. (a) Temporal evolution of F_v/F_m for ice (last cm) and water underneath the ice (depths 1.5, 10, 40 m) samples for the ice camp 2016 between 6 May and 8 July. F_v/F_m monitoring on ice samples stopped on 20 June because the chl *a* fluorescence signal was not reliable anymore. F_v/F_m monitoring on 40 and 60 m depth samples was limited between 13 May and 24 June and between 29 June and 8 July, respectively. The gray shaded area represents the range at which the algae are optimally growing. (b) The light saturation parameter, E_k , an index of photo-adaptation of the phytoplankton community, was measured at 1.5, 5 and 10 m depth. Note the log scale on the y axis.

($61 \pm 37 \mu\text{mol m}^{-2} \text{s}^{-1}$, $n = 69$), which falls in a range within the values reported in other marine studies conducted at high latitudes (Bouman et al., 2018; Massicotte et al., 2019b). The observed increase in E_k over the growing season suggests that the phytoplankton community became more photo-adapted to increasing available irradiance (Fig. 5).

4.6 Zooplankton

Zooplankton was collected from a ring net deployed under the ice at the ice camp between 22 April and 10 June in 2015 and between 16 May and 18 July in 2016. This sampler, composed of a 1 m diameter circular frame mounted with a 4 m long, 200 μm mesh size, conical plankton net was lowered cod end first to avoid filtration during the descent using an electric winch. An additional 50 μm net with an aperture of 10 cm in diameter was attached to the side

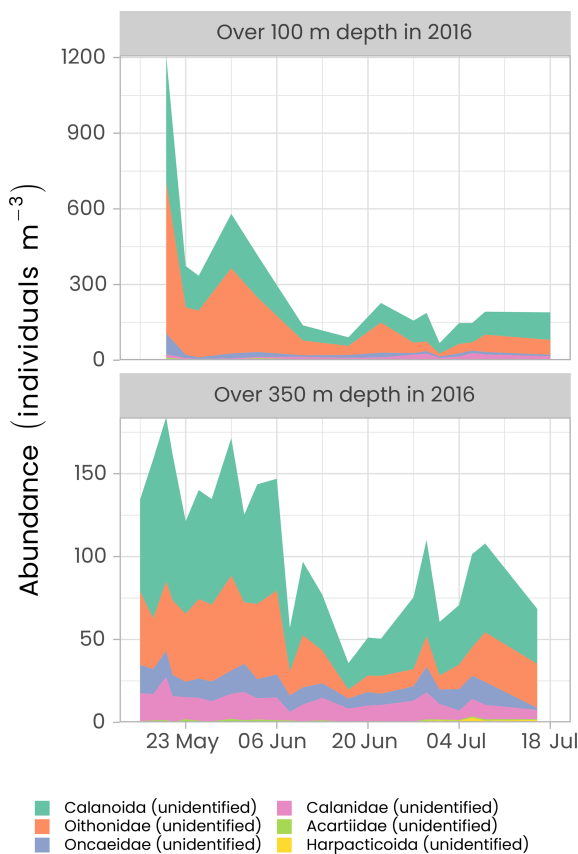


Figure 14. Time series of the abundance of the copepods (individuals per m^{-3}) measured over the first 100 and 350 m of the water column in 2016 using the ZooScan. For visualization, only the six most abundant groups are presented in decreasing order of importance. Note the different y axes in both panels.

of the metal ring to sample eggs and small zooplankton larvae, while the main net collected the mesozooplankton fraction. This sampling device was hauled vertically from a depth of 100 m (2015 and 2016) or 350 m (only in 2016), 10 m above the seafloor to the surface at a speed of about 30 m min^{-1} . The filtered volume was estimated by a KC Denmark flowmeter placed in the mouth of the $200 \mu\text{m}$ mesh net. Samples were preserved in 10 % buffered formalin seawater solution for further taxonomic analyses. Classification and count of the $200 \mu\text{m}$ mesh net samples from both campaigns were performed using the ZooScan by the PIQv team at l’Observatoire Océanographique de Villefranche-sur-Mer, France, following their protocol. Figure 14 shows the time series of the abundance of copepods (the dominant group of zooplankton in the Arctic) for the first 100 and 350 m of the water column in 2016.

The highest copepod abundance was observed in late May and early June in both the top 100 m and over the 350 m hauling depths. At the beginning of the sampling period, abundance was approximately 10 times higher in the first 100 m of the water column than over 350 m, suggesting that copepods

were agglomerating near the surface to exploit the ice algae production before the start of phytoplankton production. Abundance started to decrease during the first week of June. The family of Oithonidae and the order of Calanoida were the two most abundant groups over the two sampling depths. Oithonidae was more abundant over the top 100 m layer as this group is probably mainly composed of small epipelagic *Oithona similis*, one of the most numerous copepods in the Arctic. Calanoida, the most common copepod order, which includes the families Calanidae (including species such as *Calanus spp.*) and Acartiidae, was the dominant group over the 350 m depth haul.

4.7 Other data

An exhaustive list of all measured variables is presented in Table 2, along with contact information of principal investigators associated with each measured parameter.

5 Recommendations and lessons learned

As with any Arctic survey, a large number of measurements were acquired during the Green Edge project. Although initial recommendations on good practices about collection, processing and storage of collected data were communicated to all scientists, extensive efforts, such as data standardization, had to be performed to assemble the data. It is important for reducing possible errors that a uniformized data management plan should be prepared and distributed prior to each mission. Furthermore, dedicated data management specialists should be involved from the beginning of the project to ensure the data are adequately collected, tidied, stored, backed up and archived.

6 Code and data availability

The raw data provided by all the researchers, as well as metadata, are available on the LEFE-CYBER repository (<http://www.obs-vlfr.fr/proof/php/GREENEDGE/greenedge.php>, last access: 2 December 2019, LEFE-CYBER, 2019). The data presented in this paper and in Table 2 are hosted at SEANOE (SEA scieNtific Open data Edition) under the CC-BY license (<https://www.seanoe.org/data/00487/59892/>, last access: 2 December 2019, Massicotte et al., 2019a). Detailed metadata are associated with each file including the principal investigator’s contact information. For specific questions, please contact the principal investigator associated with the data (see Table 2).

7 Conclusions

The comprehensive dataset assembled during both Green Edge ice camp campaigns allowed us to study the fundamental physical, chemical and biological processes controlling

Table 2. Parameters measured during the Green Edge ice camp surveys. Parameters are ordered by alphabetical order and sampling year.

Year	Parameter	Sampling method	Principal investigators	Processed
2015	Absorption coefficient	In-water profiler	Guislain Bécu/Marcel Babin	Available
2015	Absorption (particulate)	Camp ice sample	Jens Ehn/Christine Cox	Available
2015	Absorption (particulate)	Camp water sample	Jens Ehn/Christine Cox	Available
2015	Absorption (particulate)	Camp ice sample	Atsushi Matsuoka/ Annick Bricaud/Joannie Ferland	Available
2015	Absorption (particulate)	Camp water sample	Atsushi Matsuoka/ Annick Bricaud/Joannie Ferland	Available
2015	ADCP (mooring)	Mooring	Claudie Marec	Available
2015	Aerosol optical depth	Surface mode	Simon Bélanger/ Clemence Goyens/ Edouard Leymarie	Available
2015	Aerosol relative humidity	Surface mode	Simon Bélanger/ Clemence Goyens/ Edouard Leymarie	Available
2015	Air relative humidity	Meteorological tower	Guillaume Massé	Available
2015	Air temperature	Meteorological tower	Guillaume Massé	Available
2015	Alkalinity total (TA)	Camp water sample	Brent Else/Jeremy Whitehead	Available
2015	Ammonium (NH_4^+)	Camp water sample	Patrick Rimbault	Data not available yet
2015	Ammonium (NH_4^+ , assimilation)	Camp water sample	Patrick Rimbault	Available
2015	Ammonium (NH_4^+ , regeneration)	Camp water sample	Patrick Rimbault	Available
2015	Angstrom coefficient	Surface mode	Simon Bélanger/ Clemence Goyens/ Edouard Leymarie	Available
2015	Attenuation coefficient	In-water profiler	Guislain Bécu/Marcel Babin	Available
2015	Backscattering coefficient	In-water profiler	Guislain Bécu/Marcel Babin	Available
2015	Bacterial sequencing	Air filtration	Rémi Amiraux	Available
2015	Bacterial sequencing	Camp water sample	Rémi Amiraux	Available
2015	Bacterial sequencing	Ice core	Rémi Amiraux	Available
2015	Bacterial sequencing	Sediment trap	Rémi Amiraux	Available
2015	Brine salinity and volume	Sea-ice core	Virginie Galindo/Søren Rysgaard	Available
2015	Chlorophyll <i>a</i>	In-water profiler	Guislain Bécu/Marcel Babin	Available
2015	Chlorophyll <i>a</i>	Sediment trap	Louis Fortier/Catherine Lalande	Available
2015	Chlorophyll <i>a</i> and phaeopigments (concentration)	Camp water sample	Marcel Babin/Joannie Ferland	Available
2015	Chlorophyll <i>a</i> and phaeopigments (concentration)	Camp water sample	Patrick Rimbault	Data not available yet
2015	Chromophoric dissolved organic matter absorption	In-water profiler	Guislain Bécu/Marcel Babin	Available
2015	Chromophoric dissolved organic matter absorption	Camp water sample	Atsushi Matsuoka/ Joannie Ferland/Marcel Babin	Available
2015	Conductivity, temperature and depth (CTD)	In-water profiler	Guislain Bécu/Marcel Babin	Available
2015	Conductivity, temperature and depth (CTD)	In-water profiler	Pascal Guillot/ Marcel Babin/Claudie Marec	Available
2015	Cryptophytes (abundance)	Camp water sample	Daniel Vaulot/Dominique Marie	Available
2015	Diffuse attenuation coefficient (Kd)	Profile mode	Guislain Bécu/Marcel Babin	Available
2015	Dimethyl sulfide (DMS)	Camp water sample	Maurice Levasseur	Available
2015	Dimethyl sulfide (DMS)	Melt pond water sample	Maurice Levasseur	Available
2015	Dimethyl sulfide (DMS)	Sea-ice core	Maurice Levasseur	Available

Table 2. Continued.

Year	Parameter	Sampling method	Principal investigators	Processed
2015	Dimethylsulfoniopropionate (DMSP)	Camp water sample	Maurice Levasseur	Available
2015	Dimethylsulfoniopropionate (DMSP)	Melt pond water sample	Maurice Levasseur	Available
2015	Dimethylsulfoniopropionate (DMSP)	Sea-ice core	Maurice Levasseur	Available
2015	Dissolved inorganic carbon (DIC)	Camp water sample	Brent Else/Jeremy Whitehead	Available
2015	Dissolved organic matter (sugars)	Rosette	Richard Sempére/ Christos Panagiotopoulos	Available
2015	Dissolved organic nitrogen (release)	Camp water sample	Patrick Raimbault	Available
2015	Downwelling irradiance	Surface mode	Simon Bélanger/ Clemence Goyens/ Edouard Leymarie	Available
2015	Downwelling irradiance above the surface ($E_d(0^+)$)	Surface mode	Marcel Babin/Martí Galí	Available
2015	Downwelling irradiance above the surface ($E_d(0^+)$)	Profile mode	Guislain Bécu/Marcel Babin	Available
2015	Downwelling irradiance ($E_d(z)$)	Profile mode	Guislain Bécu/Marcel Babin	Available
2015	$E_d(0^+)$ spectra from SBDART radiative transfer simulations	Surface mode	Marcel Babin/Martí Galí	Available
2015	Fecal pellets flux	Sediment trap	Louis Fortier/Catherine Lalande	Available
2015	Hemispherical directional reflectance distribution function	Surface mode	Simon Bélanger/ Clemence Goyens/ Edouard Leymarie	Available
2015	Hemispherical directional reflectance factor	Surface mode	Simon Bélanger/ Clemence Goyens/ Edouard Leymarie	Available
2015	Heterotrophic bacteria (abundance)	Camp water sample	Daniel Vaulot/Dominique Marie	Available
2015	Heterotrophic nanoflagellates	Camp water sample	Fabien Joux	Available
2015	Ice and snow temperature	Meteorological tower	Guillaume Massé	Available
2015	Ice thickness	Camp ice sample	Virginie Galindo/Søren Rysgaard	Available
2015	Irradiance (downwelling, upwelling)	Surface water and underwater profile mode	Lisa Matthes/Jens Ehn/ Simon Lambert-Girard/ Christopher-John Mundy	Available
2015	Isoprenoid lipids	Camp water sample	Guillaume Massé/ Caroline Guilmette	Available
2015	Isoprenoid lipids	Sea-ice core	Guillaume Massé/ Caroline Guilmette	Available
2015	Net radiation	Surface mode	Brent Else	Available
2015	Nitrate (NO_3^-)	Camp water sample	Patrick Raimbault	Available
2015	Nitrate (NO_3^-)	Sea-ice core	Patrick Raimbault	Available
2015	Nitrate (NO_3^- , assimilation)	Camp water sample	Patrick Raimbault	Available
2015	Nitrification	Camp water sample	Patrick Raimbault	Available
2015	Nitrite (NO_2^-)	Camp water sample	Patrick Raimbault	Available
2015	Nitrite (NO_2^-)	Sea-ice core	Patrick Raimbault	Available
2015	PAR from SBDART radiative transfer simulations	Surface mode	Marcel Babin/Martí Galí	Available
2015	Particle size distribution	In-water profiler	Guislain Bécu/Marcel Babin	Available
2015	Particles size	Underwater vision profiler (UVP)	Claudie Marec/Marc Picheral	Available
2015	Particulate carbon (PC)	Camp water sample	Marcel Babin/Joannie Ferland	Available

Table 2. Continued.

Year	Parameter	Sampling method	Principal investigators	Processed
2015	Particulate mass	Sediment trap	Louis Fortier/Catherine Lalande	Available
2015	Particulate nitrogen (PN)	Camp water sample	Marcel Babin/Joannie Ferland	Available
2015	Particulate nitrogen (PN)	Sediment trap	Louis Fortier/Catherine Lalande	Data not available yet
2015	Particulate organic carbon (POC)	Sediment trap	Louis Fortier/ Catherine Lalande	Available
2015	Particulate organic carbon (POC)	Camp water sample	Patrick Raimbault	Available
2015	Particulate organic nitrogen (PON)	Camp water sample	Patrick Raimbault	Available
2015	Particulate organic phosphorus (POP)	Camp water sample	Patrick Raimbault	Data not available yet
2015	PDMPO uptake	Camp water sample	Aude Leynaert	Data not available yet
2015	PDMPO uptake per species	Camp water sample	Aude Leynaert	Data not available yet
2015	Phosphate ($(\text{PO}_4)^{3-}$)	Camp water sample	Patrick Raimbault	Available
2015	Phosphate ($(\text{PO}_4)^{3-}$)	Sea-ice core	Patrick Raimbault	Available
2015	Photosynthetically available radiation (PAR)	Surface mode	Marcel Babin/Martí Galí	Available
2015	Photosynthetically available radiation (PAR)	Profile mode	Guislain Bécu/Marcel Babin	Available
2015	Photosynthetic nanoeukaryotes (abundance)	Camp water sample	Daniel Vaultot/Dominique Marie	Available
2015	Photosynthetic parameters	Camp water sample	Joannie Ferland/ Marcel Babin	Available
2015	Photosynthetic picoeukaryotes (abundance)	Camp water sample	Daniel Vaultot/Dominique Marie	Available
2015	Phytoplankton	Camp water sample	Joannie Ferland/ Pierre-Luc Grondin/ Marcel Babin/Claudie Marec	Available
2015	Phytoplankton (taxonomy)	Sediment trap	Louis Fortier/Catherine Lalande	Available
2015	Pigments	Sea-ice core	Virginie Galindo/Søren Rysgaard	Available
2015	Pigments	Camp water sample	Joséphine Ras/Hervé Claustre	Available
2015	Primary production	Camp water sample	Patrick Raimbault	Available
2015	Rrs (0^+)	Profile mode	Guislain Bécu/Marcel Babin	Available
2015	Salinity	Sea-ice core	Virginie Galindo/Søren Rysgaard	Available
2015	Salinity-induced bacterial biomarker	Ice core	Rémi Amiraux/ Jean-François Rontani	Available
2015	Salinity-induced bacterial biomarker	Sediment trap	Rémi Amiraux/ Jean-François Rontani	Available
2015	Sea-ice concentration	Surface mode	Philippe Massicotte	Available
2015	Silica biogenic (BSi)	Camp water sample	Aude Leynaert	Available
2015	Silica biogenic (BSi) dissolution rate	Camp water sample	Aude Leynaert	Available
2015	Silicate Si(OH)_4 absorption kinetics	Camp water sample	Aude Leynaert	Available
2015	Silica (uptake rate)	Camp water sample	Aude Leynaert	Available
2015	Silicate Si(OH)_4	Camp water sample	Aude Leynaert	Available
2015	Silicate Si(OH)_4	Camp water sample	Patrick Raimbault	Available
2015	Silicate Si(OH)_4	Sea-ice core	Patrick Raimbault	Available
2015	Snow depth	Camp snow sample	Virginie Galindo/Søren Rysgaard	Available
2015	Snow depth	Meteorological tower	Guillaume Massé	Available

Table 2. Continued.

Year	Parameter	Sampling method	Principal investigators	Processed
2015	Sugars	Sediment trap	Richard Sempéré/ Christos Panagiotopoulos	Available
2015	Surface albedo	Surface mode	Gauthier Verin/Ghislain Picard	Available
2015	Suspended particulate material (SPM)	Camp water sample	Marcel Babin/Joannie Ferland	Available
2015	Swimmers	Sediment trap	Louis Fortier/Catherine Lalande	Available
2015	Synechococcus (abundance)	Camp water sample	Daniel Vaulot/Dominique Marie	Available
2015	Temperature	Sea-ice core	Virginie Galindo/Søren Rysgaard	Available
2015	Total organic carbon (TOC)	Rosette	Richard Sempéré/ Christos Panagiotopoulos	Available
2015	Total organic carbon (TOC)	Camp water sample	Patrick Raimbault	Available
2015	Total organic nitrogen (TON)	Camp water sample	Patrick Raimbault	Available
2015	Total organic phosphorus (TOP)	Camp water sample	Patrick Raimbault	Available
2015	Transmittance through ice	Surface mode	Gauthier Verin	Available
2015	Under-ice export fluxes of biogenic matter (fresh)	Sediment trap	Louis Fortier/Catherine Lalande	Available
2015	Under-ice photos and video	GoPro Hero 4 on radiometer profiler	Eric Rehm	Available
2015	Upwelling irradiance ($E_u(z)$)	Profile mode	Ghislain Bécu/Marcel Babin	Available
2015	Upwelling radiance ($L_u(z)$)	Surface mode	Simon Bélanger/ Clemence Goyens/ Edouard Leymarie	Available
2015	Upwelling radiance ($L_u(z)$)	Profile mode	Ghislain Bécu/ Marcel Babin	Available
2015	Vertical profile of snow density	Surface mode	Gauthier Verin/Ghislain Picard	Available
2015	Vertical profile of specific surface area	Surface mode	Gauthier Verin/Florent Domine	Available
2015	Virus (abundance)	Camp water sample	Fabien Joux	Available
2015	Wind direction	Meteorological tower	Guillaume Massé	Available
2015	Wind speed	Meteorological tower	Guillaume Massé	Available
2015	Zooplankton (abundances)	Plankton net	Louis Fortier/Cyril Aubry	Available
2015	Zooplankton (abundances)	Plankton net (LOKI)	Louis Fortier/Cyril Aubry	Data not available yet
2015	Zooplankton (taxonomy)	Plankton net	Louis Fortier/Cyril Aubry	Available
2015	Zooplankton (taxonomy)	Plankton net (LOKI)	Louis Fortier/Cyril Aubry	Data not available yet
2015	Zooplankton vertical distribution	Underwater vision profiler (UVP)	Claudie Marec/ Sophie Renaut/Marc Picheral	Available
2016	^{234}Th (dissolved)	Rosette	Sabine Schmidt	Data not available yet
2016	^{234}Th (particulate)	Rosette	Sabine Schmidt	Data not available yet
2016	Absorption coefficient	In-water IOP profiler	Ghislain Bécu/Marcel Babin	Available
2016	Absorption (particulate)	Camp ice sample	Atsushi Matsuoka/ Annick Bricaud/ Joannie Ferland	Available
2016	Absorption (particulate)	Camp water sample	Atsushi Matsuoka/ Annick Bricaud/Joannie Ferland	Available
2016	ADCP (Mooring)	Mooring	Laurent Oziel/ Marie-Noëlle Houssais/ Marcel Babin/José Lagunas	Available
2016	Air relative humidity	Meteorological tower	Guillaume Massé	Available
2016	Air temperature	Meteorological tower	Guillaume Massé	Available
2016	Ammonium (NH_4^+)	Camp water sample	Patrick Raimbault	Data not available yet

Table 2. Continued.

Year	Parameter	Sampling method	Principal investigators	Processed
2016	Ammonium (NH_4^+ , assimilation)	Camp water sample	Patrick Raimbault	Available
2016	Ammonium (NH_4^+ , regeneration)	Camp water sample	Patrick Raimbault	Available
2016	Attenuation coefficient	In-water IOP profiler	Guislain Bécu/ Marcel Babin	Available
2016	Backscattering coefficient	In-water IOP profiler	Guislain Bécu/ Marcel Babin	Available
2016	Bacterial cultures	Camp water sample	Fabien Joux	Available
2016	Bacterial cultures	Sea-ice core	Fabien Joux	Available
2016	Bacterial production	Sea-ice core	Fabien Joux/Virginie Galindo	Available
2016	Bacterial production	Camp water sample	Fabien Joux/Virginie Galindo	Available
2016	Brine salinity and volume	Sea-ice core	Virginie Galindo/Søren Rysgaard	Available
2016	Chlorophyll <i>a</i>	In-water IOP profiler	Guislain Bécu/Marcel Babin	Available
2016	Chlorophyll <i>a</i>	Sediment trap	Louis Fortier/Catherine Lalande	Available
2016	Chlorophyll <i>a</i> and phaeopigments (concentration)	Camp water sample	Marcel Babin/Joannie Ferland	Available
2016	Chromophoric dissolved organic matter absorption	In-water IOP profiler	Guislain Bécu/Marcel Babin	Available
2016	Chromophoric dissolved organic matter absorption	Camp water sample	Atsushi Matsuoka/ Joannie Ferland/Marcel Babin	Available
2016	Chromophoric dissolved organic matter fluorescence	Camp water sample	Atsushi Matsuoka/ Joannie Ferland	Available
2016	Conductivity, temperature and depth (CTD)	In-water IOP profiler	Guislain Bécu/Marcel Babin	Available
2016	Conductivity, temperature and depth (CTD)	In-water profiler	Pascal Guillot/José Lagunas	Available
2016	Cryptophytes (abundance)	Camp water sample	Daniel Vaulot	Available
2016	Cultures of sorted populations	Camp water sample	Daniel Vaulot	Available
2016	Diatoms (Bacillariophyta) abundance	Camp water sample	Karine Leblanc/ Bernard Quéguiner/ Augustin Lafond	Available
2016	Diatoms (Bacillariophyta) taxonomy	Camp water sample	Karine Leblanc/ Bernard Quéguiner/ Augustin Lafond	Available
2016	Diffuse attenuation coefficient (Kd)	Optical radiometer profiling system	Guislain Bécu/Marcel Babin	Available
2016	Dissolved organic carbon (HTCO)	Rosette	Atsushi Matsuoka/ Ronald Benner/Joannie Ferland	Available
2016	Dissolved organic matter (Amino acids)	Rosette	Atsushi Matsuoka/ Ronald Benner/Joannie Ferland	Available
2016	Dissolved organic matter (sugars)	Rosette	Christos Panagiotopoulos/ Richard Sempéré	Available
2016	Dissolved organic nitrogen (release)	Camp water sample	Patrick Raimbault	Available
2016	Downwelling irradiance	Surface mode	Simon Bélanger/ Clemence Goyens/ Simon Lambert-Girard	Available
2016	Downwelling irradiance	Surface mode	Simon Lambert-Girard/ Edouard Leymarie	Data not available yet
2016	Downwelling irradiance above the surface ($E_d(0^+)$)	Surface mode	Marcel Babin/Martí Galí	Available
2016	Downwelling irradiance above the surface ($E_d(0^+)$)	Optical radiometer profiling system	Guislain Bécu/Marcel Babin	Available

Table 2. Continued.

Year	Parameter	Sampling method	Principal investigators	Processed
2016	Downwelling irradiance ($E_d(z)$)	Optical radiometer profiling system	Guislain Bécu/Marcel Babin	Available
2016	$E_d(0^+)$ spectra from SBDART radiative transfer simulations	Surface mode	Marcel Babin/Martí Galí	Available
2016	Fecal pellets flux	Sediment trap	Louis Fortier/Catherine Lalande	Data not available yet
2016	Hemispherical directional reflectance distribution function	Surface mode	Simon Bélanger/ Clemence Goyens/ Simon Lambert-Girard	Data not available yet
2016	Heterotrophic bacteria (abundance)	Camp water sample	Daniel Vaultot	Available
2016	Hydro SCAMP (temperature, salinity, chlorophyll, turbidity, etc.)	In-water profiler	Anda Vladoiu/ Dany Dumont/Caroline Sévigny	Available
2016	Ice and snow temperature	Meteorological tower	Guillaume Massé	Data not available yet
2016	Ice thickness	Camp ice sample	Virginie Galindo/Søren Rysgaard	Available
2016	Irradiance (downwelling)	Surface and ice-bottom mode	Lisa Matthes/Jens Ehn/ Simon Lambert-Girard/ Christopher-John Mundy	Available
2016	Irradiance (downwelling)	Under-ice irradiance transects, ROV	Lisa Matthes/ Simon Lambert-Girard/ Jens Ehn/ Christopher-John Mundy	Available
2016	Irradiance (downwelling, upwelling)	Surface water and underwater profile mode	Lisa Matthes/Jens Ehn/ Simon Lambert-Girard/ Christopher-John Mundy	Available
2016	Isoprenoid lipids	Camp water sample	Guillaume Massé/ Caroline Guilmette	Available
2016	Isoprenoid lipids	Sea-ice core	Guillaume Massé/ Caroline Guilmette	Available
2016	Lipid biomarkers	Collected organisms	Francis Dufour/ Guillaume Massé/ Pierre Ayotte/Mélanie Lemire	Available
2016	Lipid tracers of bacteria stress	Camp water sample	Jean-François Rontani/ Rémi Amiraux	Data not available yet
2016	Lipid tracers of bacteria stress	Sea-ice core	Jean-François Rontani/ Rémi Amiraux	Data not available yet
2016	Lipid tracers of bacteria stress	Sediment trap	Jean-François Rontani/ Rémi Amiraux	Data not available yet
2016	Nitrate (NO_3^-)	Camp water sample	Patrick Raimbault	Available
2016	Nitrate (NO_3^-)	Sea-ice core	Patrick Raimbault	Available
2016	Nitrate (NO_3^- , assimilation)	Camp water sample	Patrick Raimbault	Available
2016	Nitrification	Camp water sample	Patrick Raimbault	Available
2016	Nitrite (NO_2^-)	Camp water sample	Patrick Raimbault	Available
2016	Nitrite (NO_2^-)	Sea-ice core	Patrick Raimbault	Available
2016	Nutrients bioassay	Experiment	Aurelie Delaforge/ Christopher-John Mundy	Data not available yet
2016	Nutrients bioassay	Experiment	Virginie Galindo/Søren Rysgaard	Data not available yet

Table 2. Continued.

Year	Parameter	Sampling method	Principal investigators	Processed
2016	PAR from SBDART radiative transfer simulations	Surface mode	Marcel Babin/Martí Galí	Available
2016	Particle size distribution	In-water IOP profiler	Guislain Bécu/ Marcel Babin	Data not available yet
2016	Particle size distribution	In-water profiler	Lars Stemmann/José Lagunas	Data not available yet
2016	Particles size	Underwater vision profiler (UVP)	José Lagunas/Marc Picheral	Available
2016	Particulate carbon (PC)	Camp water sample	Marcel Babin/Joannie Ferland	Available
2016	Particulate mass	Sediment trap	Louis Fortier/Catherine Lalande	Available
2016	Particulate nitrogen (PN)	Camp water sample	Marcel Babin/Joannie Ferland	Available
2016	Particulate nitrogen (PN)	Sediment trap	Louis Fortier/Catherine Lalande	Data not available yet
2016	Particulate organic carbon (POC)	Sediment trap	Louis Fortier/Catherine Lalande	Available
2016	Particulate organic carbon (POC)	Camp water sample	Patrick Raimbault	Available
2016	Particulate organic nitrogen (PON)	Camp water sample	Patrick Raimbault	Available
2016	Particulate organic phosphorus (POP)	Camp water sample	Patrick Raimbault	Data not available yet
2016	PDMPO uptake	Camp water sample	Karine Leblanc/ Bernard Quéguiner	Data not available yet
2016	PDMPO uptake per species	Camp water sample	Karine Leblanc/ Bernard Quéguiner	Data not available yet
2016	Phosphate ((PO ₄) ³⁻)	Camp water sample	Patrick Raimbault	Available
2016	Phosphate ((PO ₄) ³⁻)	Sea-ice core	Patrick Raimbault	Available
2016	Photosynthetically available radiation (PAR)	Surface mode	Marcel Babin/Martí Galí	Available
2016	Photosynthetically available radiation (PAR)	Optical radiometer profiling system	Guislain Bécu/Marcel Babin	Available
2016	Photosynthetic eukaryotes (morphology)	Camp water sample	Daniel Vaultot	Data not available yet
2016	Photosynthetic nanoeukaryotes (abundance)	Camp water sample	Daniel Vaultot	Available
2016	Photosynthetic parameters	Camp water sample	Joannie Ferland/Marcel Babin	Available
2016	Photosynthetic parameters (variable fluorescence)	Camp water sample	Johann Lavaud/ Virginie Galindo/Søren Rysgaard	Available
2016	Photosynthetic parameters (variable fluorescence)	Sediment trap	Johann Lavaud/ Virginie Galindo/Søren Rysgaard	Available
2016	Photosynthetic parameters (variable fluorescence)	Sea-ice core	Johann Lavaud/ Virginie Galindo/Søren Rysgaard	Available
2016	Photosynthetic picoeukaryotes (abundance)	Camp water sample	Daniel Vaultot	Available
2016	Phytoplankton	Camp water sample	Joannie Ferland/ Pierre-Luc Grondin/ Marcel Babin	Available
2016	Phytoplankton (taxonomy)	Sediment trap	Louis Fortier/Catherine Lalande	Available
2016	Pigments	Camp water sample	Joséphine Ras/ Hervé Claustre/ Virginie Galindo/Søren Rysgaard	Available
2016	Primary production	Camp water sample	Patrick Raimbault	Available
2016	Prokaryotic diversity	Camp water sample	Fabien Joux	Data not available yet

Table 2. Continued.

Year	Parameter	Sampling method	Principal investigators	Processed
2016	Prokaryotic diversity	Sea-ice core	Fabien Joux	Data not available yet
2016	Rrs (0^+)	Optical radiometer profiling system	Guislain Béchu/Marcel Babin	Available
2016	Salinity	Sea-ice core	Virginie Galindo/Søren Rysgaard	Available
2016	Scattering coefficient	In-water IOP profiler	Guislain Béchu/Marcel Babin	Available
2016	Sea-ice concentration	Surface mode	Philippe Massicotte	Available
2016	Selenium	Collected organisms	Francis Dufour/ Guillaume Massé/ Pierre Ayotte/Mélanie Lemire	Available
2016	Silica biogenic (BSi)	Camp water sample	Aude Leynaert/ Brivaela Moriceau/ Karine Leblanc/ Bernard Quéguiner	Available
2016	Silica biogenic (BSi) dissolution rate	Camp water sample	Brivaela Moriceau	Available
2016	Silica lithogenic (LSi)	Camp water sample	Aude Leynaert/ Brivaela Moriceau/ Karine Leblanc/ Bernard Quéguiner	Data not available yet
2016	Silicate Si(OH) ₄ absorption kinetics	Camp water sample	Aude Leynaert	Available
2016	Silica (uptake rate)	Camp water sample	Aude Leynaert	Available
2016	Silicate Si(OH) ₄	Camp water sample	Aude Leynaert/ Brivaela Moriceau	Available
2016	Silicate Si(OH) ₄	Camp water sample	Patrick Raimbault	Available
2016	Silicate Si(OH) ₄	Sea-ice core	Patrick Raimbault	Available
2016	Snow depth	Camp snow sample	Virginie Galindo/Søren Rysgaard	Available
2016	Spectral downwelling radiance angular distribution	Underwater sensor	Simon Lambert-Girard/ Edouard Leymarie	Available
2016	Spectral transmittance through ice	Surface mode	Gauthier Verin/Ghislain Picard	Available
2016	Surface spectral albedo	Surface mode	Gauthier Verin/Ghislain Picard	Available
2016	Suspended particulate material (SPM)	Camp water sample	Marcel Babin/Joannie Ferland	Available
2016	Swimmers	Sediment trap	Louis Fortier/Catherine Lalande	Available
2016	Synechococcus (abundance)	Camp water sample	Daniel Vaultot	Available
2016	Temperature	Sea-ice core	Virginie Galindo/Søren Rysgaard	Available
2016	Total organic carbon (TOC)	Camp water sample	Patrick Raimbault	Available
2016	Total organic carbon (TOC) and dissolved organic carbon (DOC)	Rosette	Christos Panagiotopoulos/ Richard Sempéré	Available
2016	Total organic nitrogen (TON)	Camp water sample	Patrick Raimbault	Available
2016	Total organic phosphorus (TOP)	Camp water sample	Patrick Raimbault	Available
2016	Under-ice export fluxes of biogenic matter (fresh)	Sediment trap	Louis Fortier/Catherine Lalande	Available
2016	Upwelling irradiance ($E_u(z)$)	Optical radiometer profiling system	Guislain Béchu/Marcel Babin	Available
2016	Upwelling radiance ($L_u(z)$)	Surface mode	Simon Bélanger/ Clemence Goyens/ Simon Lambert-Girard	Data not available yet
2016	Upwelling radiance ($L_u(z)$)	Optical radiometer profiling system	Guislain Béchu/Marcel Babin	Available

Table 2. Continued.

Year	Parameter	Sampling method	Principal investigators	Processed
2016	Vertical profile of snow density	Surface mode	Gauthier Verin/Ghislain Picard	Available
2016	Vertical profile of specific surface area	Surface mode	Gauthier Verin/Florent Domine	Available
2016	Virus (abundance)	Camp water sample	Fabien Joux	Available
2016	Wind direction	Meteorological tower	Guillaume Massé	Available
2016	Wind speed	Meteorological tower	Guillaume Massé	Available
2016	Zooplankton (abundances)	Plankton net	Louis Fortier/Cyril Aubry	Available
2016	Zooplankton fecal pellet production rate	Plankton net	Louis Fortier/Makoto Sampei	Data not available yet
2016	Zooplankton grazing rate	Plankton net	Louis Fortier/Makoto Sampei	Data not available yet
2016	Zooplankton (taxonomy)	Plankton net	Louis Fortier/Cyril Aubry	Available
2016	Zooplankton vertical distribution	Underwater vision profiler (UVP)	José Lagunas/Marc Picheral	Available

the Arctic PSB. In this paper, only a handful of variables have been presented. The reader can find the complete list of measured variables in Table 2, all of which are also fully available in the data repository. Furthermore, a collection of scientific research papers is currently being submitted to a special issue of the *Elementa* journal entitled “Green Edge – The phytoplankton spring bloom in the Arctic Ocean: past, present and future response to climate variations, and impact on carbon fluxes and the marine food web”. The uniqueness and comprehensiveness of this dataset offer more opportunities to reuse it for other applications.

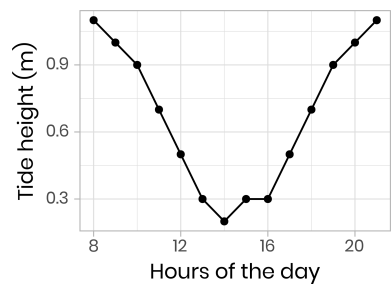
Appendix A: Surface tidal height

Figure A1. Surface tidal height vs. time at Qikiqtaarjuaq measured on 9 June 2015.

Appendix B: GoPro Hero 4 photos

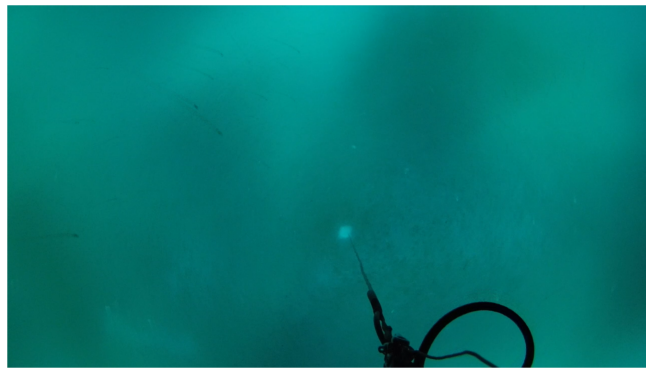


Figure B1. Video frame (00:58) from GoPro Hero 4 recording of C-OPS descent from 0 to 30 m, 18 May 2015 at the “low snow” hole. Note the streaks of nekton swimming across the upper left quadrant of the frame. Many plankton were seen in this profile, indicating an active under-ice community. A profile of the “high snow” hole on the same day, just 40 m away, showed no such plankton activity.

Table B1. Examples of GoPro Hero 4 photos at the low and high snow holes in 2015 demonstrating the spatial variability of the ice bottom across time and space.

	18 May 2015	31 May 2015	12 June 2015
Low snow			
High snow			

Author contributions. GP and LaA designed the snow optical measurements. GP participated in the 2015 campaign, along with GV, who performed the 2015 and 2016 snow-related measurements. AV, CarS and DD deployed the Self-Contained Autonomous MicroProfiler (SCAMP) on 23 June 2016 and quality-controlled, processed, analyzed and interpreted the data, with MNH adding her contribution to the analysis. GB, CIM performed the setup and deployment of the CTD inside the tent in 2015. CTD setup and deployment was performed by JosL and ChD in 2016. GB, GN, EricR, SLG, LO, JaL, JF and JuL performed the setup, calibration and deployments of the ICE-Pro optical profiler outside the tent and the IOP frame inside the tent. EricR performed the 13 h tidal cycle measurements in 2015. GN and EricR deployed the GoPro Hero on the ICE-Pro. CIM performed the setup and installation of IFCB in the lab in 2015. JF performed the setup and installation of the IFCB in the lab in 2016. JF, ErinR, AM, MHF and PLG performed the measurements. PLG analyzed the data. CIM and JosL performed the setup and deployment of an in-water profiler for particle size distribution and zooplankton vertical distribution (UVP, underwater vision profiler). CIM and JosL performed the setup and water sampling in both 2015 and 2016 campaigns. CIM was involved in the design and deployment of the ADCP in 2015, and JosL deployed the instrument in 2016. AM coordinated the sampling strategy of discrete waters in terms of examining the linkages between optical and organic matter properties. AM and AB wrote the protocols for both CDOM and particulate absorption. For CDOM, AM, JF, MHF, ErinR and PLG contributed to the measurements. For AP, AM, CéD, LL, JR, MA, HCB, BSB and TL contributed to the measurements. In 2015, particulate spectral absorption was also measured by LM, CQ and JE. NP also did snow and ice salinity and overall chl *a* filtrations in the field lab. MPA worked on tidying and uniformizing the data. MartG ran the radiative transfer calculations and compared them to irradiance measurements taken on the ice camps. LM, SLG, RH, JE, NP and CJM designed and/or carried out the TriOS and remotely operated vehicle under-ice irradiance measurements. CP and RS coordinated the sampling strategy for sugars and DOC and the analyses. RA collected the samples. Between October 2014 and July 2016, ÉB and FPdS conducted measurements, collected clams, maintained equipment, kept a time-lapse photography record and represented the Green Edge team in Qikiqtaaluk outside of the sampling season. DCS coordinated logistics in Qikiqtaaluk, in support of the 2016 ice camp. MS designed and carried out copepods incubations to collect fecal pellets out at the ice camp in 2016. MS made microscopic observations of the collected fecal pellets in the laboratory. Sea ice and snow hemispherical directional reflectance were measured on the ice camp in 2015 by SM and ClG. The setup was designed by SM, EL, SB and ClG. They also processed and analyzed the data. CatS, the LEFE-CYBER database manager is acknowledged for her help in gathering the data presented. FID designed the snow-specific surface area measurements and participated in the 2015 campaign, along with GV, who performed the 2015 and 2016 snow-related measurements. DV, ALdS, IP and PrG sampled at the ice camp for flow cytometry, phytoplankton cultures and molecular biology. CGR, ALdS, PrG and FLG established phytoplankton culture isolates. DoM and MT performed flow cytometry measurements for the 2015 and 2016 ice camp samples. DaM analyzed and plotted the flow cytometry data. FJ and VG measured the bacterial production during the 2016 ice camp.

Competing interests. The authors declare that they have no conflict of interest.

Acknowledgements. This project would not have been possible without the support of the hamlet of Qikiqtaaluk and the members of the community, as well as the Inuksuit School and its Principal Jacqueline Arsenault. The project was conducted under the scientific coordination of the Canada Excellence Research Chair in Remote Sensing of Canada's new Arctic frontier and the CNRS and Université Laval Takuvik Joint International laboratory (UMI3376). The field campaign was successful thanks to the contribution of Andrew Wells, Maxime Benoît-Gagné and Emmanuel Devred from the Takuvik laboratory, as well as Robert Hodgson from the University of Manitoba. Thanks are given to Pascale Bouruet-Aubertot and Yannis Cuypers, who provided the SCAMP and contributed to the processing, quality control, analysis and interpretation of the data. We also thank Michel Gosselin, Québec-Océan, the CCGS *Amundsen* and the Polar Continental Shelf Program for their in-kind contribution to the logistic and scientific equipment. Thanks to Etienne Ouellet for IT support and data infrastructure management. Scientific research licenses for both 2015 (NRI license 01 010 15-N-M) and 2016 (NRI license 01 001 15-R-M) were kindly accorded by the Nunavut Research Institute.

Financial support. The Green Edge project is funded by the following French and Canadian programs and agencies: ANR (contract no. 111112), CNES (project no. 131425), IPEV (project no. 1164), CSA, Fondation Total, ArcticNet, LEFE and the French Arctic Initiative (Green Edge project).

Review statement. This paper was edited by Giuseppe M. R. Manzella and reviewed by two anonymous referees.

References

- Aminot, A. and Kérout, R.: Dosage automatique des nutriments dans les eaux marines : méthodes en flux continu, Ifremer, 2007.
- Ardyna, M., Babin, M., Gosselin, M., Devred, E., Bélanger, S., Matsuoka, A., and Tremblay, J.-É.: Parameterization of vertical chlorophyll *a* in the Arctic Ocean: impact of the subsurface chlorophyll maximum on regional, seasonal, and annual primary production estimates, Biogeosciences, 10, 4383–4404, <https://doi.org/10.5194/bg-10-4383-2013>, 2013.
- Arrigo, K. R., Perovich, D. K., Pickart, R. S., Brown, Z. W., van Dijken, G. L., Lowry, K. E., Mills, M. M., Palmer, M. A., Balch, W. M., Bahr, F., Bates, N. R., Benitez-Nelson, C., Bowler, B., Brownlee, E., Ehn, J. K., Frey, K. E., Garley, R., Laney, S. R., Lubelczyk, L., Mathis, J., Matsuoka, A., Mitchell, B. G., Moore, G. W. K., Ortega-Retuerta, E., Pal, S., Polashenski, C. M., Reynolds, R. A., Schieber, B., Sosik, H. M., Stephens, M., and Swift, J. H.: Massive Phytoplankton Blooms Under Arctic Sea Ice, Science, 336, 1408–1408, <https://doi.org/10.1126/science.1215065>, 2012.
- Arrigo, K. R., Perovich, D. K., Pickart, R. S., Brown, Z. W., van Dijken, G. L., Lowry, K. E., Mills, M. M., Palmer, M. A.,

- Balch, W. M., Bates, N. R., Benitez-Nelson, C. R., Brownlee, E., Frey, K. E., Laney, S. R., Mathis, J., Matsuoka, A., Greg Mitchell, B., Moore, G., Reynolds, R. A., Sosik, H. M., and Swift, J. H.: Phytoplankton blooms beneath the sea ice in the Chukchi sea, *Deep-Sea Res. Pt. II*, 105, 1–16, <https://doi.org/10.1016/j.dsr2.2014.03.018>, 2014.
- Assmy, P., Fernández-Méndez, M., Duarte, P., Meyer, A., Randelhoff, A., Mundy, C. J., Olsen, L. M., Kauko, H. M., Bailey, A., Chierici, M., Cohen, L., Doulgeris, A. P., Ehn, J. K., Fransson, A., Gerland, S., Hop, H., Hudson, S. R., Hughes, N., Itkin, P., Johnsen, G., King, J. A., Koch, B. P., Koenig, Z., Kwasniewski, S., Laney, S. R., Nicolaus, M., Pavlov, A. K., Polashenski, C. M., Provost, C., Rösel, A., Sandbu, M., Spreen, G., Smedsrød, L. H., Sundfjord, A., Taskjelle, T., Tatarek, A., Wiktor, J., Wagner, P. M., Wold, A., Steen, H., and Granskog, M. A.: Leads in Arctic pack ice enable early phytoplankton blooms below snow-covered sea ice, *Sci. Rep.*, 7, 40850, <https://doi.org/10.1038/srep40850>, 2017.
- Bouman, H. A., Platt, T., Doblin, M., Figueiras, F. G., Gudmundsson, K., Gudfinnsson, H. G., Huang, B., Hickman, A., Hiscock, M., Jackson, T., Lutz, V. A., Mélin, F., Rey, F., Pepin, P., Segura, V., Tilstone, G. H., van Dongen-Vogels, V., and Sathyendranath, S.: Photosynthesis–irradiance parameters of marine phytoplankton: synthesis of a global data set, *Earth Syst. Sci. Data*, 10, 251–266, <https://doi.org/10.5194/essd-10-251-2018>, 2018.
- Fortier, M., Fortier, L., Michel, C., and Legendre, L.: Climatic and biological forcing of the vertical flux of biogenic particles under seasonal Arctic sea ice, *Mar. Ecol. Prog. Ser.*, 225, 1–16, <https://doi.org/10.3354/meps225001>, 2002.
- Galindo, V., Levasseur, M., Mundy, C. J., Gosselin, M., Tremblay, J.-É., Scarratt, M., Gratton, Y., Papakiriakou, T., Poulin, M., and Lizotte, M.: Biological and physical processes influencing sea ice, under-ice algae, and dimethylsulfoniopropionate during spring in the Canadian Arctic Archipelago, *J. Geophys. Res. Ocean.*, 119, 3746–3766, <https://doi.org/10.1002/2013JC009497>, 2014.
- Galindo, V., Gosselin, M., Lavaud, J., Mundy, C., Else, B., Ehn, J., Babin, M., and Rysgaard, S.: Pigment composition and photo-protection of Arctic sea ice algae during spring, *Mar. Ecol. Prog. Ser.*, 585, 49–69, <https://doi.org/10.3354/meps12398>, 2017.
- Gosselin, M., Levasseur, M., Wheeler, P. A., Horner, R. A., and Booth, B. C.: New measurements of phytoplankton and ice algal production in the Arctic Ocean, *Deep-Sea Res. Pt. II*, 44, 1623–1644, [https://doi.org/10.1016/S0967-0645\(97\)00054-4](https://doi.org/10.1016/S0967-0645(97)00054-4), 1997.
- Goyens, C., Marty, S., Leymarie, E., Antoine, D., Babin, M., and Bélanger, S.: High Angular Resolution Measurements of the Anisotropy of Reflectance of Sea Ice and Snow, *Earth Sp. Sci.*, 5, 30–47, <https://doi.org/10.1002/2017EA000332>, 2018.
- Grondin, P.-L., Ferland, J., Massicotte, P., Galindo, V., Ras, J., Claustre, H., Garcia, N., Raimbault, P., Coupel, P., Tremblay, J.-É., Forget, M.-H., Karp-Boss, L., and Babin, M.: Protists succession from ice algae to under-ice phytoplankton spring blooms in Baffin Bay, in preparation, 2019.
- Laliberté, J., Bélanger, S., and Frouin, R.: Evaluation of satellite-based algorithms to estimate photosynthetically available radiation (PAR) reaching the ocean surface at high northern latitudes, *Remote Sens. Environ.*, 184, 199–211, <https://doi.org/10.1016/j.rse.2016.06.014>, 2016.
- Laney, S. R. and Sosik, H. M.: Phytoplankton assemblage structure in and around a massive under-ice bloom in the Chukchi Sea, *Deep-Sea Res. Pt. II*, 105, 30–41, <https://doi.org/10.1016/j.dsr2.2014.03.012>, 2014.
- LEFE-CYBER: GREEN EDGE, available at: <http://www.obs-vlfr.fr/proof/php/GREENEDGE/greenedge.php>, last access: 2 December 2019.
- Letelier, R. M., Karl, D. M., Abbott, M. R., and Bidigare, R. R.: Light driven seasonal patterns of chlorophyll and nitrate in the lower euphotic zone of the North Pacific Subtropical Gyre, *Limnol. Oceanogr.*, 49, 508–519, <https://doi.org/10.4319/lo.2004.49.2.0508>, 2004.
- Leu, E., Mundy, C., Assmy, P., Campbell, K., Gabrielsen, T., Gosselin, M., Juul-Pedersen, T., and Gradinger, R.: Arctic spring awakening – Steering principles behind the phenology of vernal ice algal blooms, *Prog. Oceanogr.*, 139, 151–170, <https://doi.org/10.1016/j.pocean.2015.07.012>, 2015.
- Marie, D., Partensky, F., Jacquet, S., and Vaultor, D.: Enumeration and Cell Cycle Analysis of Natural Populations of Marine Picoplankton by Flow Cytometry Using the Nucleic Acid Stain SYBR Green I, *Appl. Environ. Microbiol.*, 63, 186–193, 1997.
- Marie, D., Rigaut-Jalabert, F., and Vaultor, D.: An improved protocol for flow cytometry analysis of phytoplankton cultures and natural samples, *Cytom. Part A*, 85, 962–968, <https://doi.org/10.1002/cyto.a.22517>, 2014.
- Massicotte, P., Bécu, G., Lambert-Girard, S., Leymarie, E., and Babin, M.: Estimating Underwater Light Regime under Spatially Heterogeneous Sea Ice in the Arctic, *Appl. Sci.*, 8, 2693, <https://doi.org/10.3390/app8122693>, 2018.
- Massicotte, P., Amiraux, R., Amyot, M.-P., Archambault, P., Ardyna, M., Arnaud, L., Artigue, L., Aubry, C., Ayotte, P., Bécu, G., Bélanger, S., Benner, R., Bittig, H. C., Bricaud, A., Brossier, É., Bruyant, F., Chauvaud, L., Christiansen-Stowe, D., Claustre, H., Cornet-Barthaux, V., Coupel, P., Cox, C., Delaforge, A., Dezutter, T., Dimier, C., Domine, F., Dufour, F., Dufresne, C., Dumont, D., Ehn, J., Else, B., Ferland, J., Forget, M.-H., Fortier, L., Galí, M., Galindo, V., Gallinari, M., Garcia, N., Gérikas-Ribeiro, C., Gourdal, M., Gourvil, P., Goyens, C., Grondin, P.-L., Guillot, P., Guilmette, C., Houssais, M.-N., Joux, F., Lacour, L., Lacour, T., Lafond, A., Lagunas, J., Lalande, C., Laliberté, J., Lambert-Girard, S., Larivière, J., Lavaud, J., Lebaron, A., Leblanc, K., Le Gall, F., Legras, J., Lemire, M., Levasseur, M., Leymarie, E., Leynaert, A., Lopes Dos Santos, A., Lourenço, A., Mah, D., Marec, C., Marie, D., Martin, N., Marty, C., Marty, S., Massé, G., Matsuoka, A., Matthes, L., Moriceau, B., Muller, P.-E., Mundy, C. J., Neukermans, G., Oziel, L., Panagiotopoulos, C., Pangazi, J.-J., Picard, G., Picheral, M., Pinczon Du Sel, F., Pogorzelec, N., Probert, I., Queguiner, B., Raimbault, P., Ras, J., Rehm, E., Reimer, E., Rontani, J.-F., Rysgaard, S., Saint-Béat, B., Sampei, M., Sansoulet, J., Schmidt, S., Sempére, R., Sévigny, C., Shen, Y., Tragin, M., Tremblay, J.-É., Vaultor, D., Verin, G., Vivier, F., Vladouli, A., Whitehead, J., and Babin, M.: The Green Edge initiative: understanding the processes controlling the under-ice Arctic phytoplankton spring bloom, SEANOE, <https://doi.org/10.17882/59892>, 2019a.
- Massicotte, P., Peeken, I., Katlein, C., Flores, H., Huot, Y., Castellani, G., Arndt, S., Lange, B. A., Tremblay, J.-É., and Babin, M.: Sensitivity of Phytoplankton Primary Production Estimates to Available Irradiance Under Heterogeneous Sea

- Ice Conditions, *J. Geophys. Res. Ocean.*, 124, 5436–5450, <https://doi.org/10.1029/2019JC015007>, 2019b.
- Matthes, L. C., Ehn, J. K., L.-Girard, S., Pogorzelec, N. M., Babin, M., and Mundy, C. J.: Average cosine coefficient and spectral distribution of the light field under sea ice: Implications for primary production, *Elem. Sci. Anth.*, 7, 25, <https://doi.org/10.1525/elementa.363>, 2019.
- Menden-Deuer, S. and Lessard, E. J.: Carbon to volume relationships for dinoflagellates, diatoms, and other protist plankton, *Limnol. Oceanogr.*, 45, 569–579, <https://doi.org/10.4319/lo.2000.45.3.0569>, 2000.
- Moberg, E. A. and Sosik, H. M.: Distance maps to estimate cell volume from two-dimensional plankton images, *Limnol. Oceanogr.-Meth.*, 10, 278–288, <https://doi.org/10.4319/lom.2012.10.278>, 2012.
- Mundy, C., Gosselin, M., Gratton, Y., Brown, K., Galindo, V., Campbell, K., Levasseur, M., Barber, D., Papakyriakou, T., and Bélanger, S.: Role of environmental factors on phytoplankton bloom initiation under landfast sea ice in Resolute Passage, Canada, *Mar. Ecol. Prog. Ser.*, 497, 39–49, <https://doi.org/10.3354/meps10587>, 2014.
- Mundy, C. J., Gosselin, M., Ehn, J., Gratton, Y., Rossnagel, A., Barber, D. G., Martin, J., Tremblay, J.-É., Palmer, M., Arrigo, K. R., Darnis, G., Fortier, L., Else, B., and Papakyriakou, T.: Contribution of under-ice primary production to an ice-edge upwelling phytoplankton bloom in the Canadian Beaufort Sea, *Geophys. Res. Lett.*, 36, L17601, <https://doi.org/10.1029/2009GL038837>, 2009.
- Olson, R. J. and Sosik, H. M.: A submersible imaging-in-flow instrument to analyze nano-and microplankton: Imaging FlowCytobot, *Limnol. Oceanogr.-Meth.*, 5, 195–203, <https://doi.org/10.4319/lom.2007.5.195>, 2007.
- Oziel, L., Massicotte, P., Randelhoff, A., Ferland, J., Vladoiu, A., Lacour, L., Galindo, V., Lambert-Girard, S., Dumont, D., Cuypers, Y., Bouruet-Aubertot, P., Mundy, C.-J., Ehn, J., Béchu, G., Marec, C., Forget, M.-H., Garcia, N., Coupel, P., Raimbault, P., Houssais, M.-N., and Babin, M.: Environmental factors influencing the seasonal dynamics of spring algal blooms in and beneath sea ice in western Baffin Bay, *Elem. Sci. Anth.*, 7, 34, <https://doi.org/10.1525/elementa.372>, 2019.
- Perrette, M., Yool, A., Quartly, G. D., and Popova, E. E.: Near-ubiquity of ice-edge blooms in the Arctic, *Biogeosciences*, 8, 515–524, <https://doi.org/10.5194/bg-8-515-2011>, 2011.
- Picheral, M., Colin, S., and Irisson, J.-O.: EcoTaxa, a tool for the taxonomic classification of images, available at: <http://ecotaxa.obs-vlfr.fr> (last access: 2 December 2019), 2017.
- Raimbault, P., Slawyk, G., Boudjellal, B., Coatanoan, C., Conan, P., Coste, B., Garcia, N., Moutin, T., and Pujo-Pay, M.: Carbon and nitrogen uptake and export in the equatorial Pacific at 150° W: Evidence of an efficient regenerated production cycle, *J. Geophys. Res.-Oceans*, 104, 3341–3356, <https://doi.org/10.1029/1998JC000004>, 1999.
- Randelhoff, A., Oziel, L., Massicotte, P., Béchu, G., Galí, M., Lacour, L., Dumont, D., Vladoiu, A., Marec, C., Bruyant, F., Houssais, M.-N., Tremblay, J.-É., Deslongchamps, G., and Babin, M.: The evolution of light and vertical mixing across a phytoplankton ice-edge bloom, *Elem. Sci. Anth.*, 7, 20, <https://doi.org/10.1525/elementa.357>, 2019.
- Ras, J., Claustre, H., and Uitz, J.: Spatial variability of phytoplankton pigment distributions in the Subtropical South Pacific Ocean: comparison between in situ and predicted data, *Biogeosciences*, 5, 353–369, <https://doi.org/10.5194/bg-5-353-2008>, 2008.
- R Core Team: R: A Language and Environment for Statistical Computing, R Foundation for Statistical Computing, Vienna, Austria, available at: <https://www.r-project.org/> (last access: 2 December 2019), 2019.
- Ricchiazzi, P., Yang, S. R., Gautier, C., and Sowle, D.: SBDART: A research and teaching software tool for plane-parallel radiative transfer in the Earth's atmosphere, *B. Am. Meteorol. Soc.*, 79, 2101–2114, 1998.
- Sakshaug, E.: Primary and Secondary Production in the Arctic Seas, in: The Organic Carbon Cycle in the Arctic Ocean, edited by: Stein, R. and MacDonald, R. W., Springer Berlin Heidelberg, Berlin, Heidelberg, 57–81, https://doi.org/10.1007/978-3-642-18912-8_3, 2004.
- Smith, R. C. and Baker, K. S.: The Analysis Of Ocean Optical Data, in: SPIE Ocean Optics VII, edited by: Blizard, M. A., vol. 489, 119, <https://doi.org/10.1117/12.943295>, 1984.
- Sosik, H. M. and Olson, R. J.: Automated taxonomic classification of phytoplankton sampled with imaging-in-flow cytometry, *Limnol. Oceanogr.-Meth.*, 5, 204–216, <https://doi.org/10.4319/lom.2007.5.204>, 2007.
- Suggett, D. J., Moore, C. M., Geider, R. J., Perkins, R. G., Kromkamp, J. C., Serôdio, J., Lavaud, J., Jesus, B., Mouget, J. L., Lefebvre, S., Forster, R. M., Suggett, D. J., Moore, C. M., Geider, R. J., Perkins, R. G., Kromkamp, J. C., Serôdio, J., Lavaud, J., Jesus, B., Mouget, J. L., Lefebvre, S., and Forster, R. M.: Chlorophyll *a* Fluorescence in Aquatic Sciences: Methods and Applications, Springer Netherlands, Dordrecht, <https://doi.org/10.1007/978-90-481-9268-7>, 2010.
- Tremblay, J.-É. and Gagnon, J.: The effects of irradiance and nutrient supply on the productivity of Arctic waters: a perspective on climate change, in: Influence of Climate Change on the Changing Arctic and Sub-Arctic Conditions, Springer Netherlands, Dordrecht, 73–93, https://doi.org/10.1007/978-1-4020-9460-6_7, 2009.
- Verin, G., Domine, F., Babin, M., Picard, G., and Arnaud, L.: Metamorphism of Arctic marine snow during the melt season. Impact on albedo, *The Cryosphere Discuss.*, <https://doi.org/10.5194/tcd-2019-113>, in review, 2019.
- Wassmann, P., Ratkova, T., Andreassen, I., Vernet, M., Pedersen, G., and Rey, F.: Spring Bloom Development in the Marginal Ice Zone and the Central Barents Sea, *Mar. Ecol.*, 20, 321–346, <https://doi.org/10.1046/j.1439-0485.1999.2034081.x>, 1999.

Remarks from the typesetter

TS1 Please check author list again. As one affiliation has been removed, affiliation numbers from 19 to 41 had to be adjusted.